NASA

Technical Memorandum 78065

High Resolution Infrared Spectroscopy: Some New Approaches and Applications to Planetary Atmospheres

Michael J. Mumma

JANUARY 1978

National Aeronautics and Space Administration

Goddard Space Flight Center
Greenbelt, Maryland 20771

HIGH RESOLUTION INFRARED SPECTROSCOPY: SOME NEW APPROACHES AND APPLICATIONS TO PLANETARY ATMOSPHERES†

Michael J. Mumma
Infrared and Radio Astronomy Branch
Laboratory for Extraterrestrial Physics
Goddard Space Flight Center
Greenbelt, Maryland 20771

ABSTRACT

Recent advances in tuneable infrared lasers and in infrared heterodyne spectroscopy enable sub-doppler spectroscopy of laboratory gases and planetary atmospheres. In this paper, the principles of spectral line formation and of techniques for retrieval of atmospheric temperature- and constituent-profiles are discussed. Applications to the atmospheres of Earth, Mars, Venus, and Jupiter are illustrated by results obtained with Fourier transform and infrared heterodyne spectrometers at resolving powers ($\lambda/\Delta\lambda$) of $\sim 10^4$ and $\sim 10^7$, respectively, showing the high complementarity of spectroscopy at these two widely different resolving powers. The principles of heterodyne spectroscopy are reviewed and its applications to atmospheric probing and to laboratory spectroscopy are discussed. Direct absorption spectroscopy with tuneable semiconductor lasers is discussed in terms of precision frequency-and line strength-measurements, showing that substantial advances in laboratory infrared spectroscopy are at hand.

†Invited paper presented at the NATO Advanced Study Institute on "Vibrational Intensities in Infrared and Raman Spectroscopy", Belgirate, Italy, Sept. 1-10, 1977.

Introduction

Planetary atmospheres derive their principal external heat input from the sun. They lose energy mainly by radiation at infrared wavelengths. Infrared spectroscopy of planetary atmospheres deals with detection of absorption and emission features from their respective constituents, leading to determinations of local physico-chemical conditions. We can estimate lower limits for the effective mean radiative temperatures of the atmospheres by writing down relations for the heat input and output and invoking equilibrium, thus

$$Q_I = \pi R^2 \int_0^\infty (1-A_\lambda) \frac{dF_s}{d\lambda} \, d\lambda \approx (1-A_v) F_s \, \pi R^2 \qquad 1)$$

and

$$Q_0 = \sigma T_e^4 \, (4\pi R^2) \qquad 2)$$

where

A_λ is the albedo at wavelength λ,

A_v is the mean visual albedo,

F_s is the solar flux at the planet's mean position,

R is the planetary radius,

σ is Stefan-Boltzmann's constant,

and T_e is the effective black-body temperature of the radiating region of the atmosphere. Eqn 2 neglects internal heat sources, and assumes a sufficiently rapid rotation rate so that radiation takes place into 4π steradians at the effective temperature, T_e. For planets having partially (Earth and Mars) or wholly (Mercury) transparent atmospheres in the infrared, some or all of the emergent radiation will come from the

surface. Eqns 1) and 2) give a zeroth order expression for the effective temperature

$$T_e \sim \left[\frac{(1-A_v)F_s}{4\sigma}\right]^{1/4} . \qquad 3)$$

Predicted and observed values of T_e are given in Table I for the major planets. Note that the observed far-infrared brightness temperatures exceed the predicted values of T_e for Jupiter, Saturn, and Neptune, showing that internal energy sources are significant for those planets.

Table I describes only the net energy budgets. More detailed analyses reveal that each atmosphere exhibits characteristic variations of kinetic temperature with altitude, the so-called vertical temperature profile. In the absence of ionization, heating, or dissociation of atmospheric molecules, the temperature should decrease with altitude according to the adiabatic lapse rate (k),

$$k = -\frac{dT}{dZ} = g/c_p \qquad 4)$$

where g is the acceleration of gravity at the reference altitude and c_p is the specific heat at constant pressure for the principal atmospheric gas[2]. Adiabatic lapse rates for various planets are: Venus (10.7 ^{o}K/km), Earth (9.8 ^{o}K/km), Mars (4.5 ^{o}K/km), and Jupiter (20 ^{o}K/km). Typical temperature profiles[3] are summarized in Fig. 1.

Heating (e.g. by absorption, ionization, and dissociation) causes additional structure on the temperature profiles. Let us examine the Earth's atmospheric temperature profile by way of illustration. Solar visual radiation penetrates to the Earth's surface, which is heated and which in turn heats the atmosphere. The temperature profile first decreases

approximately adiabatically with altitude above the surface (1 bar level), but then increases in the region where solar ultraviolet light (200-300 nm) dissociates O_3, thus forming the stratosphere. Above the stratopause, the temperature again lapses with altitude until dissociation ($\lambda \leq 200$ nm) and ionization ($\lambda \leq 100$ nm) of O_2 and N_2 inject heat into the kinetic energy distribution, forming the exosphere. Note that while the mean exospheric kinetic temperature approaches $\sim 1000\ ^{\circ}K$, the gas is not in local thermodynamic equilibrium (LTE) because the density has fallen below the level needed for collisional excitation to dominate vibrational radiative decay. Thus atmospheric sounding by infrared observations, which usually assumes LTE, is much more complicated above a certain altitude. Microwave sounding remains simple (LTE case) to higher altitudes owing to the generally much longer times for rotational relaxation.

In the case of Mars,[3b-e] the temperature follows a similar profile, except now the atmosphere is thin enough that solar ultraviolet penetrates to the surface ~~(~6mbar level), and no terrestrial-like stratosphere~~ is formed. The small temperature inversion illustrated at the 10^{-2} mbar region is thought to be caused by thermal waves[3c] propagating upward in response to the very large diurnal surface temperature variations. Mars' exospheric temperature[3d] is lower than Earth's because the dominant molecular constituent is CO_2 instead of N_2.

Venus[3f-h] (also dominantly CO_2) shows about the same exospheric temperature[3g] as Mars, however the surface temperature is $\sim 700\ ^{\circ}K$ due to the greenhouse effect. Cloud decks mantle the planet and we cannot see

below them in the infrared. These examples demonstrate that considerable contrast exists in planetary kinetic temperature profiles, which enables us to use infrared spectroscopy to probe the temperature and abundance profiles remotely.

Line Formation in Planetary Atmospheres

An external observer viewing a remote atmosphere from the top, at wavelength λ, will "see" into the medium to about one optical depth. The emergent thermal radiance at λ will be given approximately by the Planck function for the temperature (T) of that region where the optical depth is about one. Since the optical depth depends strongly on λ through the presence of spectral lines, the observer will "see" deeper into the atmosphere in regions of weak absorption, less deeply in regions of strong absorption. Then if the temperature varies with altitude, intensity contrast, i.e. spectral lines, will appear as a function of λ, and their intensity profiles may be analytically inverted for extraction of the atmospheric temperature or abundance profiles. These considerations are made quantitative in the following way.

Consider a thin slab of gas between Z_1 and Z_2 and calculate the upwelling radiance from it (Fig. 2). Neglecting cloud effects and multiple scattering, the emergent contribution from layer (L) will be[2,4]

$$dI_L = \epsilon_L(\nu,T)\ B_L\ (\nu,T(P))\ \tau_L \qquad 5)$$

where

$\epsilon_L\ (\nu,T)$ = the emissivity of the layer,

$B_L\ (\nu,T(P))$ = the Planck function at temperature (T),

τ_L = the integrated transmittance from the layer to the observer

$$\tau_L = e^{-\int K_\nu \, ndZ} = e^{-\int K_\nu du} \qquad 6)$$

where

K_ν = the absorption coefficient (cm^2) at frequency ν,

n = the number density (cm^{-3}) at height Z (cm),

u = the column density (molecules/cm^2).

The total emergent intensity will be

$$I_{TOT}(\nu) = \epsilon_S(\nu)\, B_S(\nu,T_S)\, \tau_S(\nu) + \sum_L \epsilon_L(\nu,T)\, B_L(\nu,T(P))\, \tau_L. \qquad 7)$$

The first term on the right-hand-side represents the transmitted surface contribution and the second term the summed contributions from each layer of the atmosphere. Now

$$\epsilon_L(\nu,T) = 1-\tau_L(\nu,T) \approx K_\nu \, du$$

if $\tau_L \sim 1$. Then eqn 7 can be written

$$I_{TOT}(\nu) = \epsilon_S(\nu)\, B_S(\nu,T_S)\, \tau_S(\nu) + \int_{\tau_S}^{1} B(\nu,T(P))\, d\tau \qquad 8)$$

Eqn 8 expresses the emergent spectral intensity in terms of physical parameters of the source (T_S,ϵ_S, T(Z), P(Z)). However, we really hope to determine the source parameters from the observed spectrum, i.e., given the observed intensity as a function of wavelength, and the molecular line parameters, find the atmospheric temperature profile and constituent profile by inversion of eqn 8.

For a gas which is uniformly mixed, the pressure is usually taken from

$$P = P_o\, e^{-Z/H},\quad H = \frac{kT}{mg},\ \text{the scale height} \qquad 9)$$

and the problem reduces to finding T(Z). Alternately if T(Z) is known, the partial pressure of a gas having sources and sinks (e.g. O_3 on Earth) may be determined as a function of altitude. Obviously, the quality of the inverted profile is limited by considerations such as the signal-to-noise ratio on $I_{TOT}(\nu)$, and the accuracy with which molecular line or band parameters are known.

The absorption coefficient integrated over the line is given by[5]

$$\int K_\nu\, d\nu = \frac{8\pi^3}{3hc}\ \frac{\nu\, S_{\ell u}}{g_\ell}\ N\ \frac{\exp\left(-(E_V + E_R)/kT\right)}{Q_R Q_V} \qquad 10)$$

where $S_{\ell u}$ is the quantum mechanical line strength, g_ℓ is the degeneracy of the lower state, N is the gas column density (molec/cm^2), Q_R and Q_V are the rotational and vibrational partition functions, and E_R and E_V are the rotational and vibrational energies in the lower state. The line strength is related to the transition dipole moment (μ) and the state wave functions by

$$S_{\ell u} = |\langle \Psi_u | \mu | \Psi_\ell \rangle|^2 \qquad 11)$$

The absorption coefficient at a given frequency is related to the integrated absorption coefficient by the line shape factor $b(P,T,\nu)$

$$K_\nu = b(P,T,\nu) \int K_\nu\, d\nu \qquad 12)$$

where

$$\int b(P,T,\nu)\, d\nu = 1 \text{ by definition.}$$

The exact form for $b(P,T,\nu)$ depends on the physics occurring in the medium[6]. A convenient technique for evaluating $b(P,T,\nu)$ is to divide the line into a direct contribution near line center and a wing contribution. The direct contribution is calculated from a Voigt profile (mixed Doppler and Lorentz broadening) and the wing profile is calculated from a Lorentzian. Thus near line center the line shape function is,

$$b(P,T,\nu) = \frac{1}{\alpha_D}\left(\frac{\ell n\, 2}{\pi}\right)^{1/2} \frac{y}{\pi}\int_{-\infty}^{\infty} \frac{e^{-t^2}}{y^2 + (x-t)^2}\, dt \quad , \tag{13}$$

where

$$y = \frac{\alpha_L}{\alpha_D}(\ell n\, 2)^{1/2}, \qquad x = \frac{(\nu-\nu_o)}{\alpha_D}(\ell n\, 2)^{1/2}, \tag{14}$$

and α_L and α_D are the half-widths at half maximum for Lorentz-and Doppler-broadened lines.

$$\alpha_D = 3.58 \times 10^{-7}\, \nu (T/M)^{1/2} \text{ Hz.} \tag{15}$$

The wing line shape function is calculated from

$$b(P,T,\nu) = \frac{\alpha_L}{\pi(\nu-\nu_o)^2 + \alpha_L^2} \tag{16}$$

where

$$\alpha_L = \alpha_o \left(\frac{P}{P_o}\right)\left(\frac{T_o}{T}\right)^m \tag{17}$$

where T_o and P_o are the reference temperature and pressure for which α_o was measured and $m \sim 1/2$. In this formalism, k_ν is symmetric about ν_o and therefore it does not apply when pressure induced shifts or line shape asymmetries are important. The successful inversion of eqn 8 is dependent on adequate knowledge of the molecular line parameters.

A considerably simpler calculation results when atmospheric radiance contributions can be neglected, as is the case for solar absorption measurements of telluric lines. In this case $T_S \gg T_A$ and (for weak and moderately strong lines) the relation of observed and synthetic transmittances involves only the 1st term on the RHS of eqn 9.

Applications to Planetary Atmospheres

Presuming that accurate line strengths, temperature profiles, and molecular constants exist, the expected transmittance can easily be calculated line by-line. The most comprehensive applications of this procedure have been carried out in pursuit of Fourier transform spectroscopy (FTS) or grating spectroscopy of the planets, where a very broad frequency range is measured with spectral resolution ~ 1 cm^{-1} to ~ 0.1 cm^{-1}. An example is given in Fig 3 where the measured Venusian spectrum is compared with the calculated synthetic spectrum from 750 - 1000 cm^{-1} for a model which includes lines of CO_2 and a H_2SO_4 haze.[7a] Agreement between the observed and synthetic transmittances is impressive. The spectral resolution is sufficient to resolve the bands into individual ro-vibrational lines, but it is not sufficient to resolve the intensity profiles of individual lines. Thus inversion can only be carried out for very strong bands, e.g. in the Q-branch of CO_2 at 791 cm^{-1} and the 667 cm^{-1} ν_2 fundamental.

An entirely new class of physical information is obtained when lines are measured at sub-doppler resolution. Townes and his co-workers[8]

first observed lines of the 10.6μm bands of CO_2 on Venus with an infrared heterodyne spectrometer (IRHS) and discovered that although the effective continuum temperature in this region is ~ 230K (see Fig. 3), the center of the lines contained an emission feature which came up to ~300 K brightness temperature. The kinetic width of the feature corresponded to a temperature of ~ 180 K indicating that some non-thermal pump was operating. They invoked absorption of solar radiation in ν_3, $3\nu_3$,... with optical trapping and subsequent cascade in the ν_3-$2\nu_2$ band to explain the non-thermal emission. Observations made by our group indicate that for some lines the central emission peak consists of a combination of thermally radiant and non-thermally radiant contributions (Fig. 4). Inversion of the thermally radiant portion, using the techniques described earlier, indicates a mesospheric temperature inversion[3h] in the 10^{-2} to 10^{-4} mbar region (see also Fig. 1).

Precise measurements of the doppler shifts of these narrow features have been used by Betz et al[9a] to derive wind velocities in the high altitude regions (80 km) where these lines are formed. The derived values are ~ 10 m/sec retrograde, much smaller than the ~ 100 m/sec velocities derived for lower altitudes from Pepsios measurements by Traub and Carleton,[10] and independently from the ultraviolet cloud motion studies of Mariner 10.[11] Recent measurements on $^{13}C^{16}O_2$ lines, formed deeper in the Cytherean atmosphere, are in good agreement with the Pepsios results.[9b]

FTS provides broad simultaneous wavelength coverage at moderate spectral resolving power while IRHS provides narrow simultaneous wavelength coverage at very high resolving power. As illustrated by the Cytherean results,

FTS and IRHS are complementary techniques which together can provide a very complete picture of the spectroscopy and physics involved.

The complementarity of FTS and IRHS is further illustrated by observations of Mars. The atmosphere of Mars consists of CO_2, N_2, Ar, various isotopic variants and other trace species (Table II). The Mariner 9 spacecraft carried an FTS into orbit about the planet in 1971 and infrared spectra were measured from 2000 - 200 cm^{-1} at $\sim$ 2 cm^{-1} resolution over a period of many months. An average of 1747 spectra is compared with the synthetic spectrum[7b] in Fig 5. Bands of CO_2, H_2O, and silicates are evident in the spectra. Maguire[12] has derived upper limits for minor constituents from these data (Table II). While the $\nu_3 - 2\nu_2$ (10.6μm) bands are barely visible on this plot scale, a heterodyne spectrum of the P14 line shows remarkably deep and narrow lines with a non-thermal emission spike at line center (Betz et al[8], Fig. 6). Inversion of the 15μm CO_2 (ν_2) band in the IRIS spectra allowed extraction of temperature profiles from the surface to $\sim$ 50 km. Temperature fields were measured for nearly the entire planet, from which global winds were determined[7b].

Principles of Heterodyne Spectroscopy

The techniques and advantages of interferometric spectrometers are widely understood, but infrared heterodyne spectroscopy is relatively new. It is an extremely powerful tool worthy of some detailed discussion. The concepts and much of the instrumentation are borrowed from radio astronomy where heterodyning has been used for decades.

Infrared heterodyne detection is achieved by allowing radiation from a coherent local oscillator (field, $E_o\ e^{i\omega_o t}$) and from a source (field, $E_s\ e^{i\omega_s t}$) to illuminate a non-linear detector (photo-mixer). Classically, the total local field is

$$E = E_o\ e^{i\omega_o t} + E_s\ e^{i\omega_s t}, \tag{18}$$

and the electrical signal output is

$$E^* E = E_o^*\ E_o + E_s^*\ E_s + 2E_o\ E_s \cos\ (\omega_o - \omega_s)\ t \tag{19}$$

where the cross-term is the instantaneous IF heterodyne signal, and

$$\omega_o - \omega_s = \omega_{IF} \tag{20}$$

is the intermediate frequency. The relation between the source spectrum and the IF spectrum is shown in Fig. 7.

For a given local oscillator frequency, a range of source frequencies in the upper and lower detector sidebands will be efficiently mixed and will give corresponding IF signals. The upper limit to this range of IF frequencies is set by the frequency roll-off of the detector/pre-amplifier response. For the best HgCdTe detectors, this can be in excess of ~1.5 GHz.[13] The sidebands are folded at the IF and so a given rf filter contains contributions from both-upper and lower sidebands (Fig. 7). The slope of the continuum is greatly exaggerated in Fig. 7; at these high resolving powers the continuum is essentially flat. A multiplex advantage is obtained by simultaneously sampling the IF range with a set of consecutive rf filters (so-called filter bank) as described later. The source spectrum is measured simultaneously over some frequency range (~ 1000 MHz) by the filter bank. Tuning the rf local oscillator positions the filter bank with respect to the zero

of IF. Spectral scanning over ranges wider than the detector bandwidth requires a tuneable infrared local oscillator.

If the IF is passed through a radio frequency filter of bandwidth B (Hz), then passed through a second square law detector and time-averaged for time τ (sec), the noise equivalent spectral intensity in the shot-noise limit will be given by

$$NEF = \frac{\Delta}{\sqrt{B\tau}} \quad \frac{\text{photons}}{\text{sec Hz}} \tag{21}$$

where Δ is the total degradation factor due to system losses. The various losses are discussed in detail elsewhere.[14,15] Careful attention to details of the optical and electronic design can result in $\Delta \leq 25$ at the present time. The system discussed in this paper[14] has a measured $\Delta = 27$.

Molecules in local thermodynamic equilibrium (LTE) cannot radiate intensities (photons/sec Hz) greater than the Planck function for that temperature, corresponding to the optically thick case. Absorption lines are normally measured against some continuum black- or grey-body emitter such as the sun (telluric lines), planetary surface (e.g. Mars, Fig. 5), atmospheric continuum (e.g. Venus, Fig. 3), or laboratory black-body source (gas cell measurements). Thus, for both absorption and emission, detection of the Planck function provides a good measure of the practical usefulness of heterodyne detection. The spectral radiance (photons/sec Hz cm^2 sr) of a black-body is given by

$$R = \frac{2}{\lambda^2 (e^{h\nu/kT} - 1)} \quad \frac{\text{photons}}{\text{sec Hz cm}^2 \text{ sr}} \tag{22}$$

The etendue of heterodyne receivers has been discussed in detail by Siegman[16] who showed that

$$A_e \, \Omega_A \sim \lambda^2, \tag{23}$$

the so-called antenna theorem. A_e is the effective aperture and Ω_A is the beam solid angle defined as in usual antenna theory. The principal advantage of using telescopic optics is thus to decrease the field-of-view, i.e., for viewing spatially small source regions, and heterodyne receivers are usually matched to the diffraction limited field-of-view. According to eqn's 22 and 23, the spectral intensity (F) collected in the heterodyne field-of-view is

$$F = \frac{2}{e^{h\nu/kT} - 1} \quad \frac{\text{photons}}{\text{sec Hz}} \qquad 24)$$

This spectral intensity is shown in Fig. 8 for various black-body source temperatures. The limit, S/N = 3, is shown for experimental parameters $\Delta_T = 27$, B = 25 MHz, and τ = 400 sec and indicates the range of temperatures for which heterodyne spectroscopy is sufficiently sensitive to measure atmospheric lines at sub-doppler resolutions with reasonable integration times.

Some provision for wavelength tuning is needed in order to do spectroscopy. Continuously tuneable lasers are most desireable since a particular molecular line can then be preselected for study on the basis of line strength, spectral purity, and minimum dependence on rotational temperature, and the line can be optimally positioned in the filter bank. In addition, a tuneable infrared laser and a single channel receiver can be used as a tuneable spectrometer directly. This has the advantage of reducing sideband overlap problems but the multiplex advantage is lost. Grating tuned gas lasers enable selected wavelength intervals to be measured and, if care is exercised in choosing the

laser transition, remote sensing of some molecules having lines within $\sim$ 2 GHz of the laser transition is possible. Semiconductor diode lasers appear to exhibit considerable promise for use as local oscillators, but so far have only been used in two cases for field measurements.[17,18] Their output wavelength can be composition tuned to a particular spectral region and then fine-tuned by current, heat sink temperature, or magnetic field variation.[19] Representative tuning ranges are illustrated in Fig. 9 (after Ref. 19), however sufficient power for local oscillator use is available only over a much more restricted range.

The optical and electronic design characteristics of the Goddard Space Flight Center CO_2 laser heterodyne spectrometer[14] are illustrated in Fig. 10. Two modes of operation are shown - the remote sensing and the laboratory mode. In the remote sensing mode, signal (S) from a telescope is chopped against a reference (R, a calibrated black body, cold source, or sky) with a bow tie mirror chopper. The load chopper is used only for calibration and for atmospheric observation. For astronomical observations (planets, stars, nebulae) the sky chopper is used to switch the beam $\sim$ 1 arc minute off the source every other half cycle. The chopping frequency is 23 Hz. The signal beam is combined with a matched CO_2 laser local oscillator beam at the IR beamsplitter and then both beams are focused onto a HgCdTe photomixer with a telescope-matching lens. The IF difference frequencies are amplified and fed into the spectral line receiver where integration and synchronous detection take place. For astronomical viewing, visible - IR beamsplitters at the telescope output and at the IR detector permit visual guiding and

alignment using crossline reticles and eye-pieces. The laboratory mode of operation is utilized for fundamental measurements of line-center frequencies, line-shape parameters, and line strengths. In this case, the signal beam views a suitable reference while the radiation from a black body source is focussed through a sample gas cell (NH_3 in Fig 10), superimposing absorption lines on the continuum. The remaining optical paths and operation of the system are identical to the remote sensing mode and an absorption line can be observed (see Fig 11). Line center frequencies for 11 lines of NH_3 (ν_2) in close overlap with CO_2 laser transitions have been measured in this way[20] (Table III) and used to improve the accuracy of the inversion splitting constants for the $\nu_2 = 1$ level.[21] As we shall see, these accurate line frequencies also enabled a search for Jovian auroral emissions in the ν_2-band.

Laboratory Absorption Spectroscopy with Tuneable Semi-conductor Lasers

While absolute line strengths, line shapes, and line broadening parameters may be measured with a heterodyne spectrometer, it is often more convenient to use a tuneable laser as an active source for direct absorption experiments. Two principal problems exist in using tuneable lasers for intensity, line shape, and line frequency measurements. The first relates to intensity measurements. The precision with which line intensities may be measured is about $1:10^4$, however the accuracy of quantum mechanical line strengths is limited by the accuracy with which the gas column density is known. The cell length may be known to very

high precision, in which case the absolute pressure measurement limits the accuracy of absolute experimental line strengths. Relative line strengths can be measured directly to $1:10^4$ without knowledge of the column density, and such precision intensity measurements on fully-resolved lines will be a major advance in infrared spectroscopy. The second problem in direct absorption measurements is that of frequency calibration, for which heterodyning provides a very accurate measure of line frequencies. Accuracies of $\pm$ 1 MHz are routinely possible, and accuracies of $\pm$ 100 kHz are feasible using Lamb-dip stabilization.

A laboratory system utilizing heterodyne frequency calibration is illustrated in Fig. 12. In principle, both the CO_2 laser and the diode laser could be separately Lamb-dip stabilized, but in practice the diodes available so far do not have sufficient power to saturate the transition in the experimental gas. The tuning range of a single diode laser used in our laboratory is indicated in Fig. 13. Frequency stabilization to $\sim$5 MHz is achieved by temperature control[22] and vibration isolation[23]. Spectroscopic studies of C_3O_2, CF_2Cl_2, NH_3, and H_2O_2 are presently underway in our lab. An example of a Q-region (923 cm^{-1}) of CF_2Cl_2 is shown in Fig. 14. The etalon transmission fringes below give a first order calibration good to $\sim$ 30 MHz ($\sim 10^{-3}$ cm^{-1}). In the past few years, many papers have been published of high resolution spectra using TDL's, but relatively few have deduced molecular constants from the data. A list of reduced spectra is given in Table IV.

Further Applications to Planetary Spectroscopy

With this background in the experimental aspects of heterodyne spectroscopy, let us examine further applications to planetary atmospheres. As mentioned earlier, solar absorption measurements of Telluric lines can be carried out at much higher signal-to-noise ratio than self-emission studies due to the higher source brightness. Observed (FTS) and synthetic transmittances of some telluric lines are shown in Fig. 15.[7a] The model in this case included a line by-line calculation for a multiple layered atmosphere consisting of CO_2, O_3, H_2O, N_2O, and CH_4. Heterodyne measurements of the atmospheric R8 line of CO_2 near 10.3μm are shown in Fig. 16.[24] The measured line profile was inverted[22] using the known temperature profile and resulted in an altitude profile for CO_2 which is uniformly mixed to ~ 50 km at a volume mixing ratio of $\sim 3 \times 10^{-4}$, in good agreement with independent results. The returned altitude profile was then used to model the R8 atmospheric line, with the results shown in Fig. 16. Similar modelling has been carried out[24] to determine the accuracy with which vertical profiles of O_3 can be retrieved from heterodyne measurements, with the results shown in Fig. 17. An interesting criterion is the minimum detectable mixing ratio for trace constituents in the earth's stratosphere. The minimum detectable column density (optically thin case) is given by

$$U_{min} = \frac{(NEF)_{Het}}{k_\nu B_\nu (T_{solar})} \; ; \; U_{min} \sim q^\nu_{min} U_T \qquad 25)$$

where q is the mixing ratio, and U_T is the total gas column density

along the path. Taking B = 5 MHz τ = 1000 sec, and Δ = 30, with a 20 km path length, $k_o \sim 50$ for $S \sim 1$ cm^{-1} (cm atm)$^{-1}$, we have for the minimum detectable mixing ratio (q^v_{min})

$$q^v_{min} \sim 2 \times 10^{-12}. \qquad 26)$$

This detection limit is compared with the abundances of some stratospheric minor constituents in Fig. 18. The detection limit may be lowered by $\sim$ 20 if nearly horizontal viewing paths are used.

Turning finally to the planet Jupiter, those molecules known to exist in the Jovian atmosphere are listed in Table II. Because of the low atmospheric temperatures, heterodyne detection of atmospheric thermal lines is difficult. However, Jupiter is known to have extensive radiation belts and shows extensive decametric radio activity, modulated somehow by one of its moons, Io. Precipitating electrons should give rise to non-thermal NH_3 auroral emissions if sufficiently energetic ($\sim$ 1 Mev) electrons penetrate to levels where NH_3 exists in copious quantities. A search for non-thermal NH_3 emission was rewarded by clear evidence for detection of auroral emissions[25] (Fig. 19). The evidence is strong: (1) two transitions of NH_3 were detected, (2) the excitation temperature is much greater than the kinetic temperature, (3) the emission is seen only from the polar regions, (4) tuning the rf oscillator shifts the line, (5) the lines were detected at the correct doppler shifted frequencies. Evidence for detection of microwave emission of CH_4 in coincidence with decametric activity was also recently reported by Fox and Jennings.[26]

Summary

Fourier transform spectroscopy and infrared heterodyne spectroscopy are highly complementary tools for remotely probing planetary atmospheres. Because the spectral resolving powers are widely different, the two techniques probe different altitude regions of the atmosphere and together can provide a more complete determination of the physics and chemistry. The use of CO_2-based heterodyne spectrometers for sub-doppler planetary spectroscopy has already provided insights into an additional class of physical phenomena. Tuneable infrared local oscillators will enable the full power of heterodyne spectroscopy to be applied to these problems. Tuneable semiconductor lasers have made absorption spectroscopy at a spectral resolution of 10^{-4} cm^{-1} a routine laboratory tool. Infrared spectroscopy is thus moving into new domains, offering the opportunity for substantially eliminating experimental uncertainty in line positions with a concomitant increase in accuracy of absolute intensities and of molecular constants.

REFERENCES

1a) C.W. Allen, Astrophysical Quantities, 3rd ed, Athlune Press Univ. of London, (1973).

b) R.L. Newburn and S. Gulkis,"A Survey of the Outer Planets Jupiter, Saturn, Uranus, Neptune, Pluto, and Their Satellites", Spa. Sci. Rev. 3, 179 (1973).

1c) T.H. Van Der Haar and V.E. Suomi, "Measurements of the Earth's Radiation Budget from Satellites During A Five-Year Period. Part I: Extended Time and Space Means", J. Atmos. Sci. 28, 305 (1971).

1d) E.L. Wright, "Recalibration of Far-Infrared Brightness Temperatures of the Planets", Ap.J. 210, 250 (1976).

1e) R.F. Loewenstein, D.A. Harper, S.H. Mosely, C.M. Telesco, H.A. Thronson, R.H. Hildebrand, S.E. Whitcomb, R. Winston, and R.F. Stiening, "Far-IR and Sub-mm Observations of the Planets", Icarus 31, 315 (1977).

1f) R.F. Loewenstein, D.A. Harper, and H. Mosely, "The Effective Temperature of Neptune", Ap.J. (Letters) 218, L145 (1977).

1g) S.C. Chase, E.D. Miner, D. Morrison, G. Munch, and G. Neugebauer, "Mariner 10 Infrared Radiometer Results: Temperatures and Thermal Properties of the Surface of Mercury", Icarus 28, 565 (1976).

2) cf. R.M. Goody, Atmospheric Radiation, Oxford Clarendon Press (1964), also R.M. Goody and J.C.G. Walker, Atmospheres, Prentice-Hall Inc. (1972).

3) Representative temperature profiles taken from the following references:

Earth: 3a) U.S. Standard Atmosphere, 1976, NOAA-S/T 76-1562 (U.S. Govt Printing Office) (1976).

Mars: 3b) R. Hanel, B. Conrath, W. Hovis, V. Kunde, P. Lowman, W. Maguire, J. Pearl, J. Pirraglia, C. Prabhakara, B. Schlachman, G. Levin, P. Straat and T. Burke, "Investigation of the Martian Environment by Infrared Spectroscopy on Mariner 9", Icarus 17, 423 (1972).

3c) R.W. Zurek, "Diurnal Tide in the Martian Atmosphere", J. Atmos. Sci. 33, 321 (1976).

3d) D.J. Strickland, A.I. Stewart, C.A. Barth, and C.W. Hord, "Mariner 9 Ultraviolet Spectrometer Experiment: Mars Atomic Oxygen 1304-Å Emission", J. Geophys. Res. 78, 4547 (1973).

3e) A.O. Nier, W.B. Hanson, A. Sieff, M.B. McElroy, N.W. Spencer, R.J. Duckett, T.C.D. Knight and W.S. Cook, "Composition and Structure of the Martian Atmosphere: Preliminary results from Viking I," Science 193, 4255 (1976).

Venus: 3f) H.T. Howard, G.L. Tyler, G. Fjeldbo, A.J. Kliore, G.S. Levy, D.L. Brunn, R. Dickinson, R.E. Edelson, W.L. Martin, R.B. Postal, B. Seidel, T.T. Sesplaukis, D.L. Shirley, C.T. Stelzried, D.N. Sweetnam, A.I. Zygielbaum, P.B. Esposito, J.D. Anderson, I.I. Shapiro, and D.R. Reasenberg, "Venus: Mass, Gravity Field, Atmosphere, and Ionosphere as measured by the Mariner 10 Dual-Frequency Radio System", Science 183, 1297 (1974).

3g) A.L. Broadfoot, S. Kumar, M.J.S. Belton, and M.B. McElroy, "Ultraviolet Observations of Venus from Mariner 10: Preliminary Results", Science 183, 1315 (1974).

3h) R.E. Dickinson, "Venus Mesosphere and Thermosphere Temperature Structure", Icarus 27, 479 (1976).

Jupiter 3i) A.J. Kliore, P.M. Woiceshyn, and W.B. Hubbard, "Temperature of the atmosphere of Jupiter from Pioneer 10/11 radio occultations", Geophys. Res. Letters 3, 113 (1976).

4) J.T. Houghton and F.W. Taylor, "Remote Sounding from Artificial Satellites and Space Probes of the Atmospheres of the Earth and Planets", Rep. Prog. Phys. 36, 827 (1973).

5) G. Herzberg, Molecular Spectra and Molecular Structure, II. Infrared and Raman Spectra of Polyatomic Molecules, Van Nostrand Reinhold Co. (1945).

6) A.C.G. Mitchell and M.W. Zemansky, Resonance Radiation and Excited Atoms, Cambridge University Press (1971).

7a) V.G. Kunde, R.A. Hanel, and L.W. Herath, "High Spectral Resolution Groundbased Observations of Venus in the 450-1250 cm^{-1} Region", Icarus 32, 210 (1977).

7b) For a general review of Fourier Transform Spectroscopy of the planets, see R.A. Hanel and V.G. Kunde, "Fourier Spectroscopy in Planetary Research", Spa. Sci. Rev. 18, 201 (1975).

8) Betz, A.L., R.A. McLaren, E.C. Sutton and M.A. Johnson, "Infrared Heterodyne Spectroscopy of CO_2 in the Atmosphere of Mars", Icarus 30, 650 (1977). See also M.A. Johnson, A.L. Betz, B.A. McLaren, E.C. Sutton and C.H. Townes, "Non-thermal 10μm CO_2 Lines in the Atmospheres of Mars and Venus", Astrophys. J. 208, L145-L148 (1976).

9a) A.L. Betz, M.A. Johnson, R.A. McLaren, and E.C. Sutton, "Heterodyne Detection of CO_2 Emission Lines and Wind Velocities in the Atmosphere of Venus", Ap.J. (Letters) 208, L141 (1976).

9b) Betz, A.L., E.C. Sutton, R.A. McLaren, and C.W. McAlary, "Laser Heterodyne Spectroscopy", Roy. Soc. Can. - Symp. on Planet, Atmos. (1977), Ottawa, Canada (to be published).

10) W.A. Traub and N.P. Carleton, "Spectroscopic Observations of Winds on Venus", J. Atmos. Sci 32, 1045 (1975).

11) B.C. Murray, M.J.S. Belton, G.E. Danielson, M.E. Davies, D. Gault, B. Hapke, B. O'Leary, R.G. Strom, V. Suomi, and N. Trask, "Venus:Atmospheric Motion and Structure from Mariner 10 Pictures", Science 183, 1307 (1974).

12) W.C. Maguire, "Martian Isotopic Ratios and Upper Limits for Possible Minor Constituents as Derived from Mariner 9 Infrared Spectrometer Data", Icarus 32, 85 (1977).

13) D.L. Spears, "Planar HgCdTe Quadrantal Heterodyne Arrays with GHz Response at 10.6μm", Infrared Physics, 17, 5(1977).

14) M.J. Mumma, T. Kostiuk, and D. Buhl, "A 10μm Laser Heterodyne Spectrometer for Remote Detection of Trace Gases", Optical Engineering 17, xxxx (1977).

15) M.M. Abbas, M.J. Mumma, T. Kostiuk, and D. Buhl, "Sensitivity Limits of an Infrared Heterodyne Spectrometer for Astrophysical Applications", Applied Optics 15, 427 (1976).

16) A. E. Siegman, "The Antenna Properties of Optical Heterodyne Receivers", Proc. IEEE 54, 1350 (1966).

17) M. Mumma, T. Kostiuk, S. Cohen, D. Buhl, and P.C. von Thuna, "Infrared Heterodyne Spectroscopy of Astronomical and Laboratory Sources at 8.5μm", Nature 253, 514 (1975).

18) M.A. Frerking and D.J. Muelhner, "Infrared Heterodyne Spectroscopy of Atmospheric Ozone", Applied Optics 16, 526 (1977).

19) I. Melngailis and A. Mooradian, "Tuneable Semiconductor Lasers and Applications", in Physics of Quantum Electronics, Vol. 2: Laser Applications to Optics and Spectroscopy, ed. S.F. Jacobs, M. Sargent III, J.F. Scott, and M.O. Scully, Addison Wesley (1975).

20) J.J. Hillman, T. Kostiuk, D. Buhl, J. Faris, J.C. Novaco, and M.J. Mumma, "Precision Measurements of NH_3 Spectral Lines Near 11μm Using the Infrared Heterodyne Technique", Optics Letters 1, 81 (1977).

21) J.J. Hillman, T. Kostiuk, and M.J. Mumma, "Inversion Splitting in the ν_2 State of Ammonia", J. Molec. Spectrosc. (to be submitted).

22) D.E. Jennings and J.J. Hillman, "Active Thermal Compensation for Diode Laser Stabilization on Closed-Cycle Refrigerators", Rev. Sci. Instrum. 48, xxxx (1977).

23) D.E. Jennings and J.J. Hillman, "Shock Isolator for Diode Laser Operation on a Closed-Cycle Refrigerator", Rev. Sci. Instrum. 48, xxxx (1977).

24) M.M. Abbas, V. Kunde, and M.J. Mumma, "Infrared Heterodyne Spectroscopy of the Earth's Stratosphere", submitted to J. Atmos. Sciences (1977).

25) T. Kostiuk, M.J. Mumma, J.J. Hillman, D. Buhl, L.W. Brown, J. Faris, and D.L. Spears, "NH_3 Spectral Line Measurements on Earth and Jupiter using a 10μm Superheterodyne Receiver", Infrared Physics (in press, 1977).

26) K. Fox and D.E. Jennings, "Possible Jovian Methane Emission at 76 GHz in Coincidence with Decametric Activity", Ap.J. 216, L83 (1977).

27) cf. K. Fox, "High Resolution Infrared Spectroscopy of Planetary Atmospheres", in Molecular Spectroscopy: Modern Research, ed. K.N. Rao and C.W. Mathews, Academic Press (1972), and references cited therein.

28) See the collected initial results of the Viking 1 and 2 Mars landing experiments contained in Science 193, No. 4255 (1976); 194, No. 4260 (1976); and 194, No. 4271 (1976).

29) For a review see S.T. Ridgeway, H.P. Larson, and U. Fink, "The Infrared Spectrum of Jupiter", in Jupiter, ed. T. Gehrels, Univ. of Ariz. Press, Tucson, Ariz (1976), p. 384.

30) W.H. Weber, J.P. Aldridge, H. Flicker, N.G. Nereson, H. Filip, and M.J. Reisfeld, "High-Resolution Spectra of the $\nu_2 + \nu_7$ Bands of C_3O_2 in the 12μm Region", J. Mol. Spectrosc. 65, 474 (1977).

31) C.W. Peters, W.H. Weber, and P.D. Maker, "The Infrared Spectrum of C_3O_2: The Interaction between ν_7 and the ν_2 and ν_4 Vibrations", J. Mol. Spectrosc. 66, 133 (1977).

32) R.T. Menzies, J.S. Margolis, E.D. Hinkley, and R.A. Toth, "Measurement of the Fundamental Vibration-Rotation Spectrum of ClO", Applied Optics 16, 523 (1977).

33) J.P. Sattler and G.J. Simonis, "Tunable Diode Laser Spectroscopy of Methyl Fluoride", J. Quant. Elect. EQ-13, 461 (1977).

34) J.P. Sattler and R.K. Ritter, "Diode Laser Spectra of NH_3 in the 9.5μm Region", J. Molec. Spectrosc. (in press, 1977).

35) J.P. Aldridge, H. Filip, H. Flicker, R.F. Holland, R.S. McDowell, N.G. Nereson, and K. Fox: "Octahedral Fine-Structure Splittings in ν_3 of SF_6", J. Mol. Spectrosc. 58, 165 (1975).

36) E.D. Hinkley, A.R. Calawa, P.L. Kelley and S.A. Clough, "Tunable-Laser Spectroscopy of the ν_1 Band of SO_2", J. Appl. Phys. 43, 3222 (1972).

37) Preliminary results of molecular band analyses have been carried out for these molecules:

a) "Coriolis Splitting Constant for UF_6 from Laser Diode Spectroscopy", J.P. Aldridge, H. Filip, H. Galbraith, R.S. McDowell, D.F. Smith, and K. Fox, LASL Conference on Lasers for Isotope Separation, Albuquerque, NM, April 13-14, 1976.

b) "High Resolution Spectrum of ν_3 of OsO_4," K. Fox, R.S. McDowell, N. G. Nereson, B.J. Krohn, and R.C. Kennedy, Ohio State University Molecular Spectroscopy Symposium, Columbus, Ohio, June 13-17, 1977, Abstract RA6.

c) "High Resolution Spectra of Sixteen Q Branches in the ν_9 Fundamental of Ethane," H. Flicker, R.S. McDowell, N.G. Nereson and K. Fox, ibid., Abstract TB5.

d) "Laser Spectroscopy of ν_4 of Methane, " K. Fox, J.P. Aldridge, H.J. Flicker, R.F. Holland, R.S. McDowell, and N.G. Nereson, Ohio State University Molecular Spectroscopy Conference, Columbus, Ohio, June 16-20, 1975.

38) The author acknowledges contributions of his colleagues to some of the work presented here: theoretical discussions with Dr. M. M. Abbas (GSFC and Univ. of Md.) and Dr. Virgil Kunde (GSFC), experimental assistance from Dr. T. Kostiuk and Dr. D. Buhl, and assistance by Dr. D. Jennings. The author thanks Dr.'s Abbas, J.J. Hillman and D. Jennings for permission to include figures taken from publications in press or in preparation, and Dr. K. Fox (Univ. of Tenn.) for helpful suggestions on the manuscript.

Table I

EFFECTIVE TEMPERATURES

Planet	Mean Distance from sun (10^6 km)	Local Solar Flux 10^6 erg $cm^{-2}s^{-1}$	Albedo	Effective Temperature (K) Predicted[d]	Observed	Ref
Mercury	57.9	9.08	0.056[a]	525[e]	h	1g
Venus	108.2	2.59	0.72[a]	238	240±8	1d
Earth	149.6	1.36	0.30[b]	254.5	254.3	1b
Mars	227.9	.59	0.16[a]	228	~228[f]	1d
Jupiter	778.3	.050	0.45[c]	105	127±3	1d
Saturn	1427.0	.015	0.61[c]	71	85±2	1d
Uranus	2869.6	.0037	0.35[c]	68-57[g]	58±2	1e
Neptune	4496.6	.0015	0.35[c]	45	55.5±2.3	1f
Pluto	5900	.00087	0.145[a]	42	--	

a) Ref 1a.

b) Ref 1c.

c) Ref. 1b and references cited therein.

d) Eqn. 3, $\sigma = 5.67 \times 10^{-5}$ erg cm^{-2} K^{-4} sec^{-1}

e) Calculated assuming reradiation from one hemisphere only, because of Mercury's unusually slow rotation and lack of atmosphere. Mercury's orbital eccentricity is very large, leading to commensurate variations in T_e.

f) Mars' large orbital eccentricity causes a significant variation in effective temperature over an orbital period. The observed temperatures satisfy $T_e \sim 282R^{-1/2}$, where R is the Mars-Sun distance in A.U. and 1 A.U. is the mean Earth-Sun distance.

g) Uranus' rotation axis lies nearly in the ecliptic plane, therefore the effective reradiating surface may vary from only one hemisphere to a full sphere as the planet moves 90° along its orbit.

h) Far infrared observations show general agreement with predictions, but the measured effective temperatures vary greatly since the ground-based observer never sees the full sunlit hemisphere. Infrared measurements on the Mariner 10 spacecraft showed the surface temperature to be ~100K at local midnight (Ref 1g).

Table II

Atmospheric Composition of the Planets

Venus	
CO_2 (dominant, ~ 100%)	Ref. 27
CO, HCl, HF, H_2O	Ref. 27
H_2SO_4	Ref. 7a
Mars	
$^{12}CO_2$ 95%, N_2 2.6%, Ar^{40} 1.6%, O_2 0.15%	Ref. 3b, 28
$^{13}CO_2$, $^{12}C^{16}O^{18}O$, $^{12}C^{17}O^{16}O$	Ref. 3b, 28
Ar^{36}, Kr, Xe, N^{14}/N^{15}, Ar^{40}/Ar^{36}	Ref. 27
H_2O, CO	
O_3 (uv detection)	
Upper Limits for:	
C_2H_2, C_2H_4, C_2H_6, CH_4, N_2O, NO_2, NH_3, PH_3, SO_2, OCS,	Ref. 12
H_2S, NO	Ref. 12
Earth	
N_2 78.1%, O_2 20.9%, Ar 0.9,	
CO_2, O_3, SO_2, NO_2, CH_4, N_2O, H_2O	Ref. 3a
NH_3, CO, H_2O_2, HCl, ClO, F11, F12, ...	Ref. 3a
Jupiter	
H_2 (vis), He (inferred)	
NH_3, CH_4	Ref. 29
C_2H_2, C_2H_6, H_2O, HD, CH_3D, PH_3, $^{13}CH_4$, GeH_4, CO, HCN	Ref. 29

TABLE III

Line Center Frequencies of Selected ν_2 NH_3 Transitions

NH_3 TRANSITION	PREVIOUS RESULTS[a] cm^{-1}	HETERODYNE RESULTS[a] cm^{-1}
aR(1,1)	971.88204±0.0001	971.88224±0.00007
sQ(2,2)	967.73859±0.0001	967.73841±0.00007
aQ(2,2)	931.3336±0.001	931.33342±0.00012
sP(4,3)	887.8782±0.005	887.87683±0.00012
sQ(5,4)	966.26931±0.0001	966.26935±0.00012
aQ(5,3)	932.99243±0.0001	932.99226±0.00012
aQ(6,4)	932.6343±0.005	932.63582±0.00030
aQ(6,6)	927.3234±0.001	927.32323±0.00012
sQ(14,13)	954.5812±0.005	954.57840±0.00034
2sQ(1,1)	949.4462±0.005	949.44732±0.00007
2sQ(6,3)	938.7282±0.005	938.72850±0.00015

a) See ref 20 and references cited thereim

Table IV

MOLECULAR BAND ANALYSES

USING TUNABLE DIODE LASERS

Molecule	Band	Frequency	Reference
C_3O_2	$\nu_2 + \nu_7$	830 cm^{-1}	30
C_3O_2	ν_2, ν_4, ν_7	1580	31
ClO	ν_1	850	32
CH_3F	ν_3	1050	33
NH_3	ν_2	1000	34
SF_6	ν_3	950	35
SO_2	ν_1	1150	36

$UF_6(\nu_3)$, $OsO_4(\nu_3)$, $C_2H_6(\nu_9)$, and $CH_4(\nu_4)$ - Preliminary Analysis only, see ref. 37.

LIST OF FIGURES

Fig. 1 Representative kinetic temperature profiles for Venus, Earth, Mars, and Jupiter.

Fig. 2 Formation of spectral lines in a multi-layered atmosphere.

Fig. 3 Thermal emission spectrum of Venus after Kunde et al[7a]. The spectrum was measured with a Fourier transform spectrometer at 0.2 cm^{-1} resolution. A broad absorption near 900 cm^{-1} is attributed to H_2SO_4 haze and all lines are due to various bands of CO_2. A computed synthetic spectrum is shown displaced by 20 ^{o}K for clarity. The line marked R8 is shown in Fig. 4 at higher resolution.

Fig. 4 Intensity profile of the Venusian R8 line of CO_2 in the 10.4μm band. The spectrum was measured with an infrared heterodyne spectrometer at 0.00016 cm^{-1} resolution. The brightness temperature at line center is ~ 310 ^{o}K and the symmetric structure near line center is thought to originate in two physically distant processes as discussed in the text.

Fig. 5 Average of 1747 FTS spectra of Mars taken by the IRIS experiment on the Mariner 9 Mars orbiting spacecraft (Hanel et al[7b]). The synthetic spectrum is displaced for clarity.

Fig. 6 Infrared heterodyne measurement of the P(14) line of CO_2 in the 10.4μm band (after Betz et al[8]). The solid curve is the synthetic profile expected for an atmosphere having 4.8 mbar surface pressure and a 2 $^{o}K/Km$ lapse rate. The non-thermal peak at line center is attributed to solar pumping in the near infrared[8].

Fig. 7 The relation between the source and intermediate frequency spectra in heterodyne detection. Hypothetical absorption or emission lines are shown superimposed on a thermal continuum with greatly exaggerated slope. At these resolving powers ($\lambda/\Delta\lambda \sim 10^7$) the continuum has essentially constant intensity. Signals in the upper and lower sideband are folded with respect to the local oscillator frequency and their sum is detected. The width of an individual filter is indicated by B.

Fig. 8 The spectral intensities of black-body sources which fill the etendue ($A\Omega \sim \lambda^2$) of a heterodyne receiver are shown as a function of wavelength. The intensities shown include both modes of polarization. The sensitivity limit for S/N = 3 is shown for a present generation CO_2 system (9-11μm). Diode laser local oscillators should enable extension to the entire wavelength range shown here.

Fig. 9 Compositions of various semiconductor diode lasers and the wavelength ranges over which lasing has been achieved (solid bars, after Melngailis and Mooradian[19]). Dashed bars indicate the expected extension of lasing action.

Fig. 10 Optical and electronic block diagram of the GSFC CO_2 laser heterodyne spectrometer. The reference black body provides intensity calibration and a bright background source for measuring absorption lines in gas cells. Either of two choppers is used, depending on the observational mode. Principles of operation are discussed in the text.

Fig. 11 An example of a fully resolved molecular line profile (NH_3 SQ(5,4) measured with the system shown in Fig. 10. The line is measured on the left at 5 MHz resolution and on the right at 50 MHz resolution. Calibration is achieved by dividing the measured spectrum by one taken with an empty gas cell.

Fig. 12 Schematic of a tuneable semiconductor diode laser absorption spectrometer. The diode laser is cooled by a closed-cycle helium refrigerator, and a single spectral mode is selected by a grating. Etalon fringes are superimposed for rough frequency calibration, and precise frequency calibration is achieved by heterodyning against a lamb-dip stabilized CO_2 laser.

Fig. 13 The tuning range of one semiconductor laser in frequency-current-temperature space. The extreme versatility of this widely tuneable device is indicated by the various gases having fundamental bands within the tuning range.

Fig. 14 An example of semi-conductor laser absorption spectra measured with the system shown in Fig. 12. The etalon fringes are shown in the lowest trace, the absorption spectrum of CF_2Cl_2 in the middle trace, and the incident laser intensity in the top trace (after Jennings, private communication).

Fig. 15 Solar absorption spectrum of the terrestrial atmosphere measured with an FTS instrument (Kunde et al[7a]). The synthetic spectrum is displaced for clarity.

Fig. 16 Intensity profile of a terrestrial line (R8 of CO_2) measured with the heterodyne spectrometer shown in Fig. 10. The profile reveals pressure broadened wings and a high altitude doppler core. Inversion of the observed line shape allowed extraction of the volume mixing ratio for CO_2 up to 50 Km[24].

Fig. 17 Results of synthetic profile analysis for retrieval of altitude profiles of O_3. A line profile was calculated from the assumed altitude profile (solid line), and was then inverted to recover the altitude profile shown by the broken line.[24] The initial guess used in the inversion process is indicated.

Fig. 18 Detection limit for terrestrial atmospheric species by heterodyne spectroscopy in the solar absorption mode, compared with modelled volume mixing ratio profiles for some important trace species. Assumptions are given in the text. Further improvement of $\sim$ 20 in sensitivity is gained by observing at nearly horizontal paths

Fig. 19 Detection of non-thermal NH_3 aR(1,1) emission from the north polar region of Jupiter.[23] The expected line position after correcting for planetary doppler shifts is indicated by the arrow. The rf local oscillator was tuned between the two spectra by 100 MHz, and the NH_3 line shifted accordingly. The two filter banks did not overlap at this time.

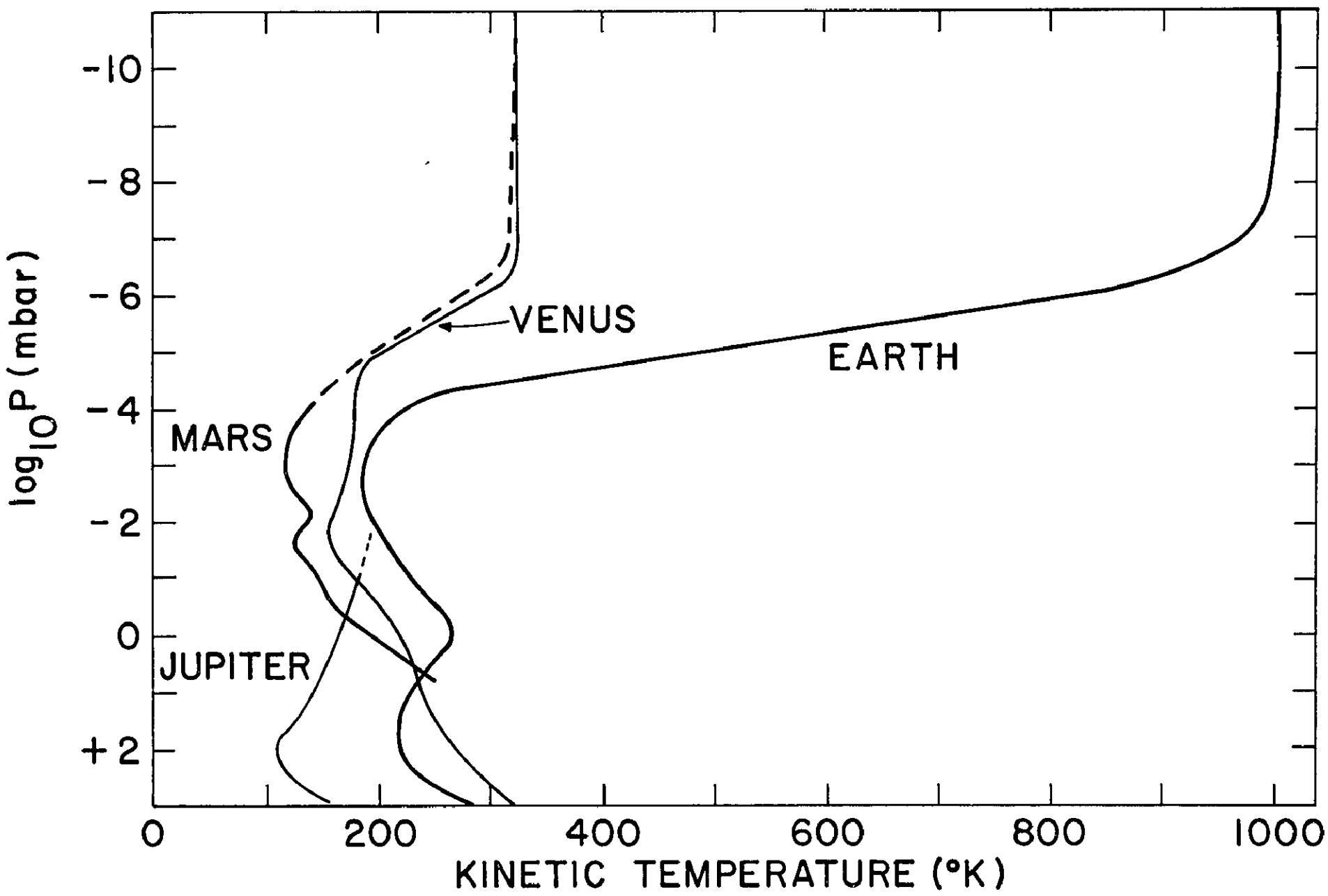
-10
-8
-6
-4
-2
0
+2
log10P (mbar)
VENUS
EARTH
MARS
JUPITER
0
200
400
600
800
1000
KINETIC TEMPERATURE (°K)

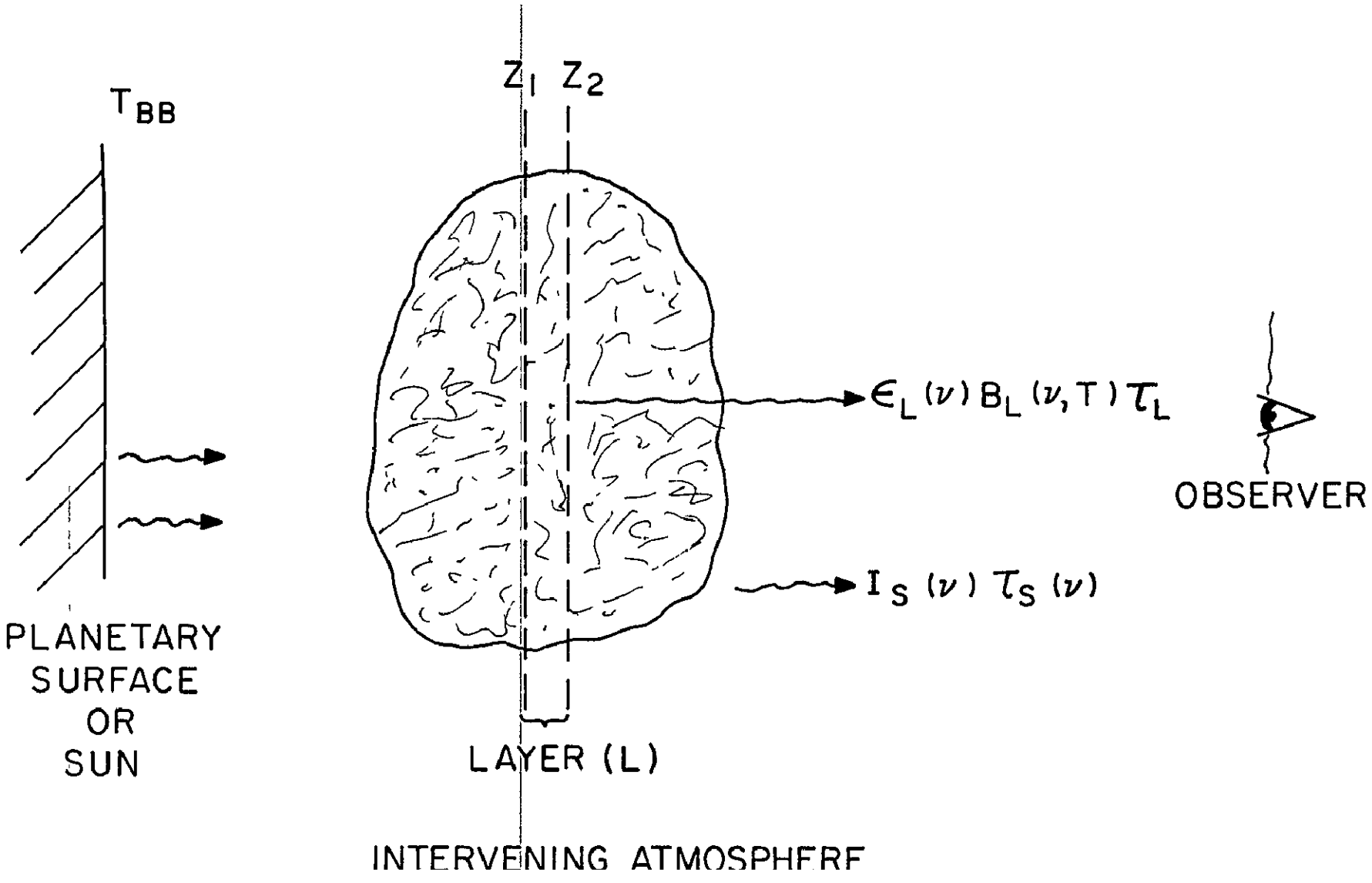
T_{BB}
Z_1 Z_2
$\epsilon_L(\nu)\, B_L(\nu, T)\, \tau_L$
OBSERVER
$I_S(\nu)\, \tau_S(\nu)$
PLANETARY SURFACE OR SUN
LAYER (L)
INTERVENING ATMOSPHERE

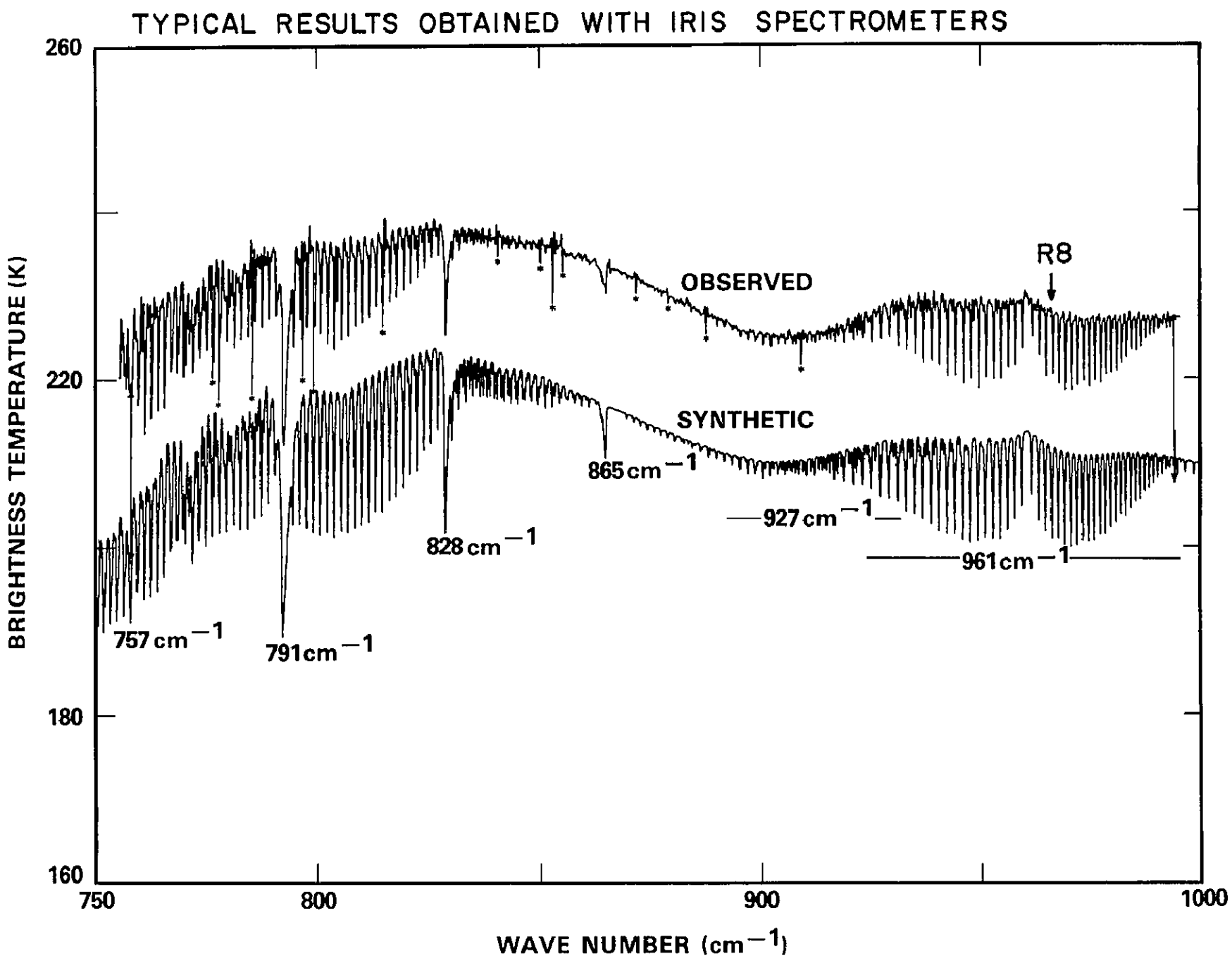
TYPICAL RESULTS OBTAINED WITH IRIS SPECTROMETERS
260
220
180
160
BRIGHTNESS TEMPERATURE (K)
750
800
900
1000
WAVE NUMBER (cm⁻¹)
OBSERVED
SYNTHETIC
R8
757 cm⁻¹
791 cm⁻¹
828 cm⁻¹
865 cm⁻¹
927 cm⁻¹
961 cm⁻¹

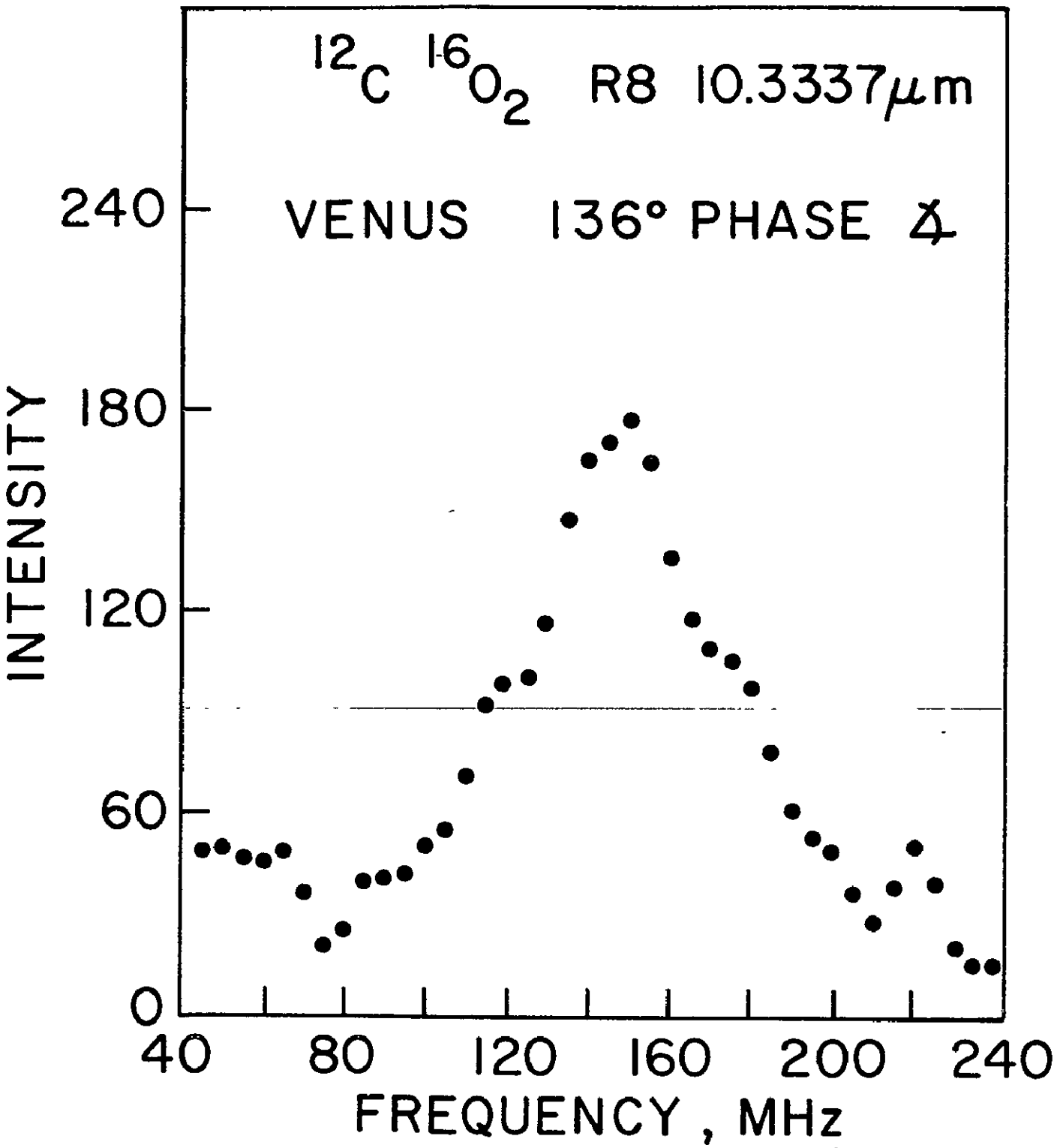
$^{12}C\ ^{16}O_2$ R8 10.3337μm
VENUS 136° PHASE Δ
INTENSITY
240
180
120
60
0
40
80
120
160
200
240
FREQUENCY, MHz

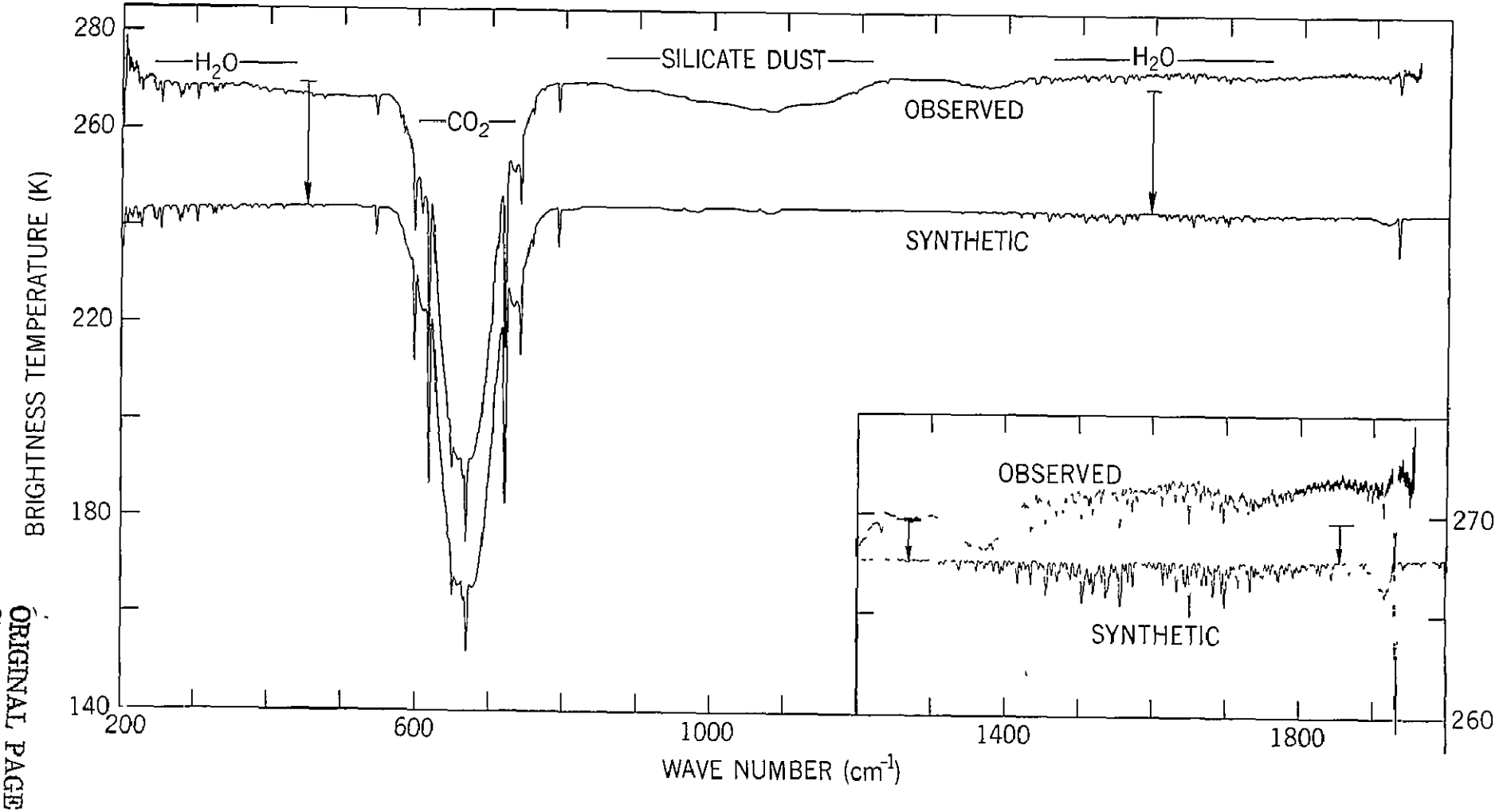

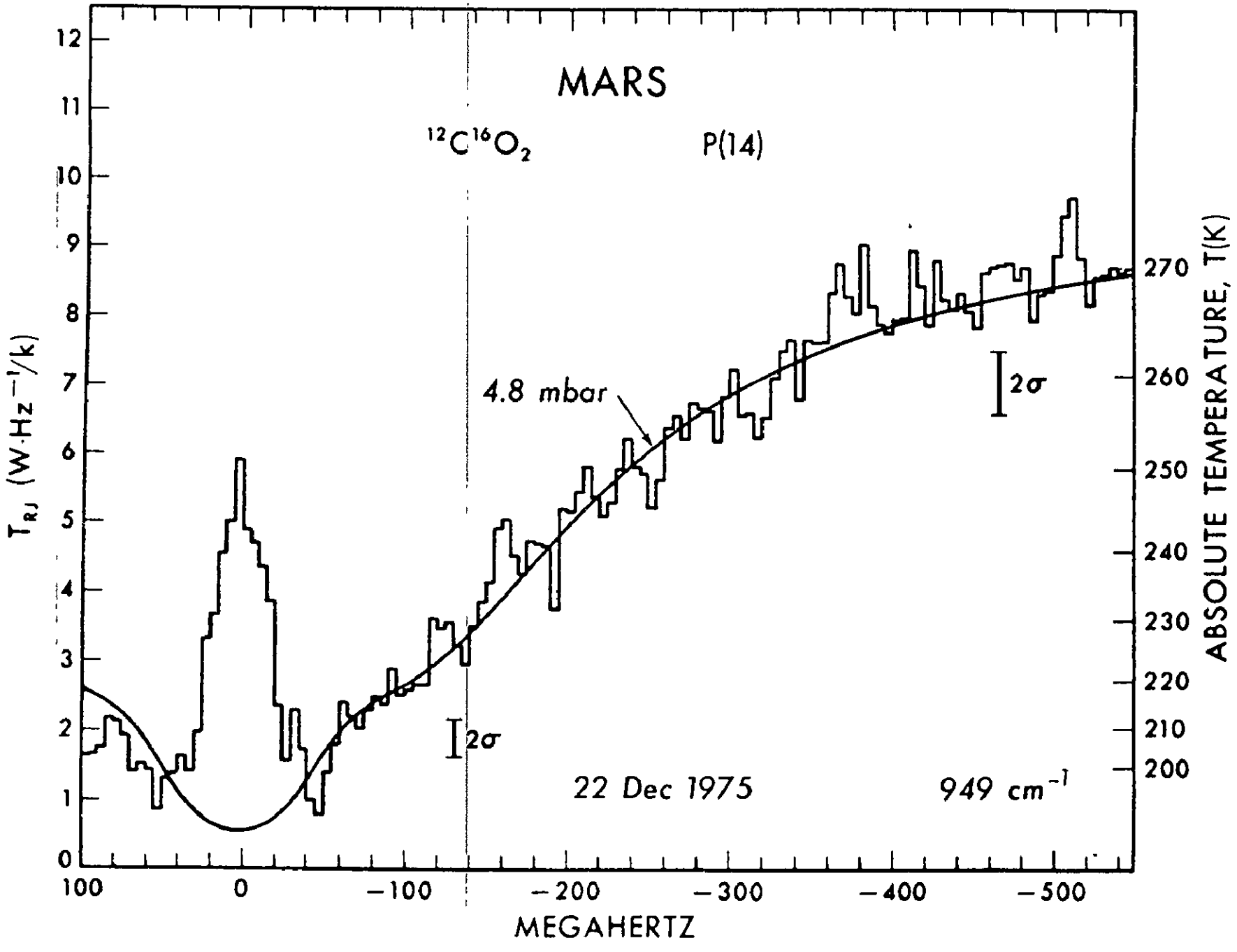
MARS
$^{12}C^{16}O_2$ P(14)
4.8 mbar
2σ
2σ
22 Dec 1975
949 cm^{-1}
T_{RJ} (W·Hz^{-1}/k)
ABSOLUTE TEMPERATURE, T(K)
MEGAHERTZ
12
11
10
9
8
7
6
5
4
3
2
1
0
270
260
250
240
230
220
210
200
100
0
−100
−200
−300
−400
−500

DOUBLE SIDE-BAND DETECTION:

RELATION BETWEEN SOURCE AND IF SPECTRA

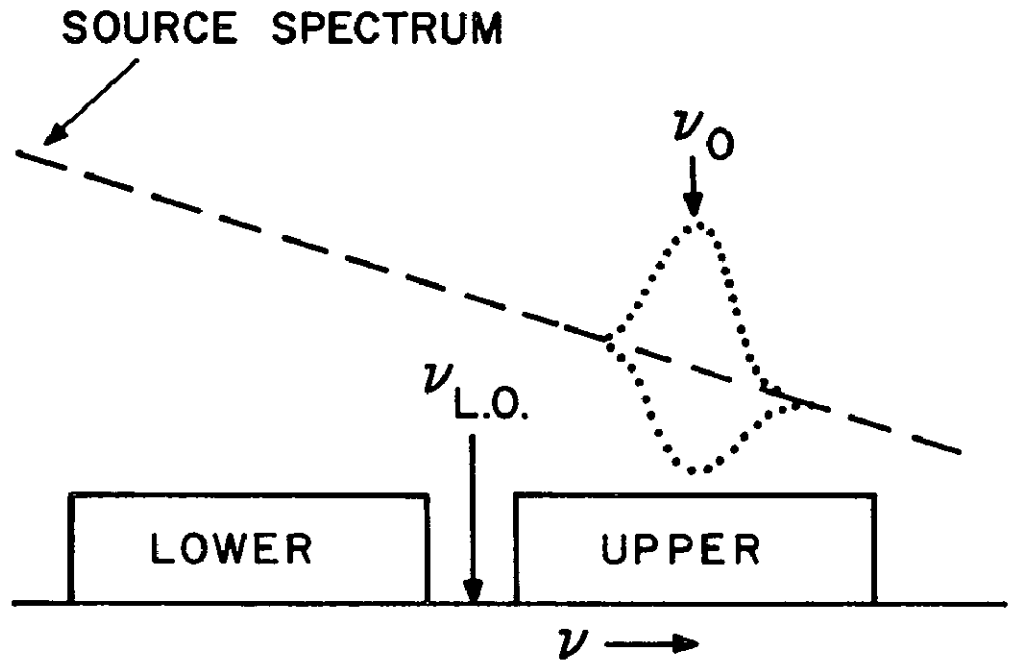

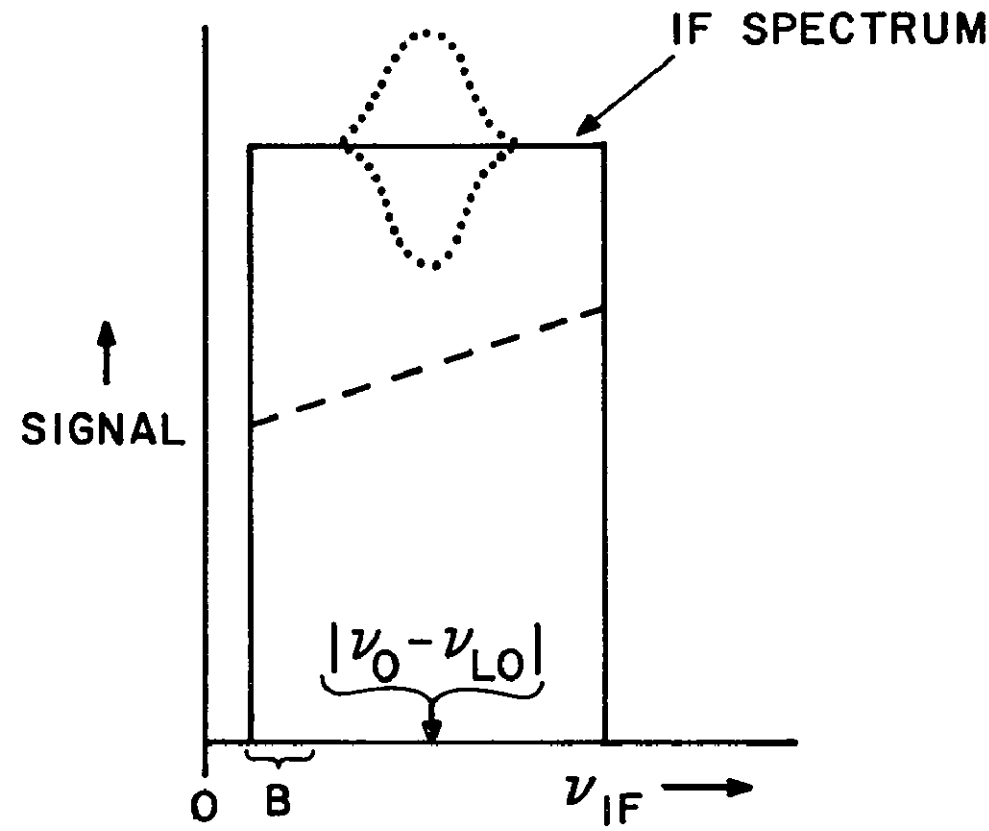

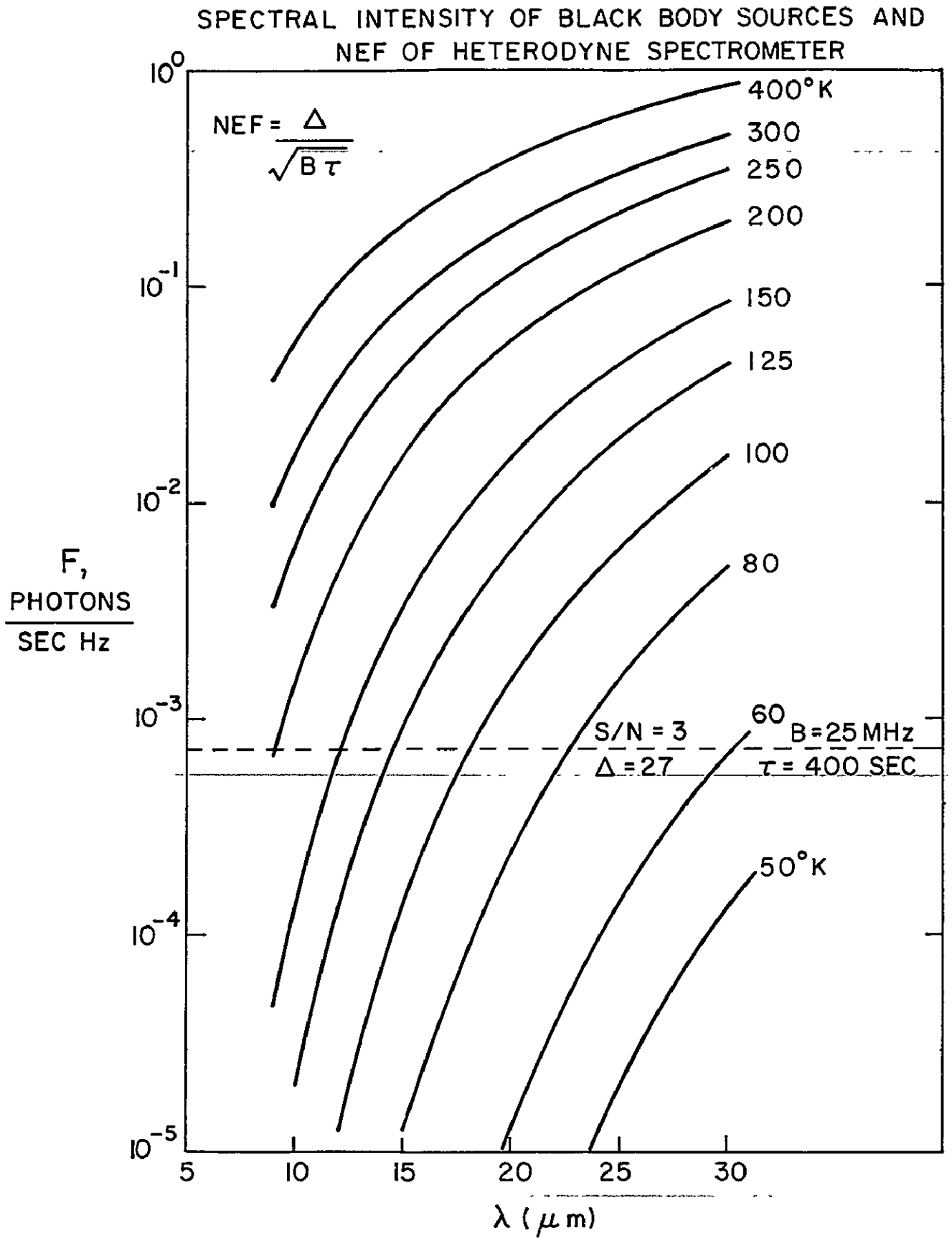
SPECTRAL INTENSITY OF BLACK BODY SOURCES AND
NEF OF HETERODYNE SPECTROMETER
NEF = Δ / √(B τ)
400°K
300
250
200
150
125
100
80
60
50°K
S/N = 3
Δ = 27
B = 25 MHz
τ = 400 SEC
F, PHOTONS / SEC Hz
λ (μm)
10^0
10^-1
10^-2
10^-3
10^-4
10^-5
5
10
15
20
25
30

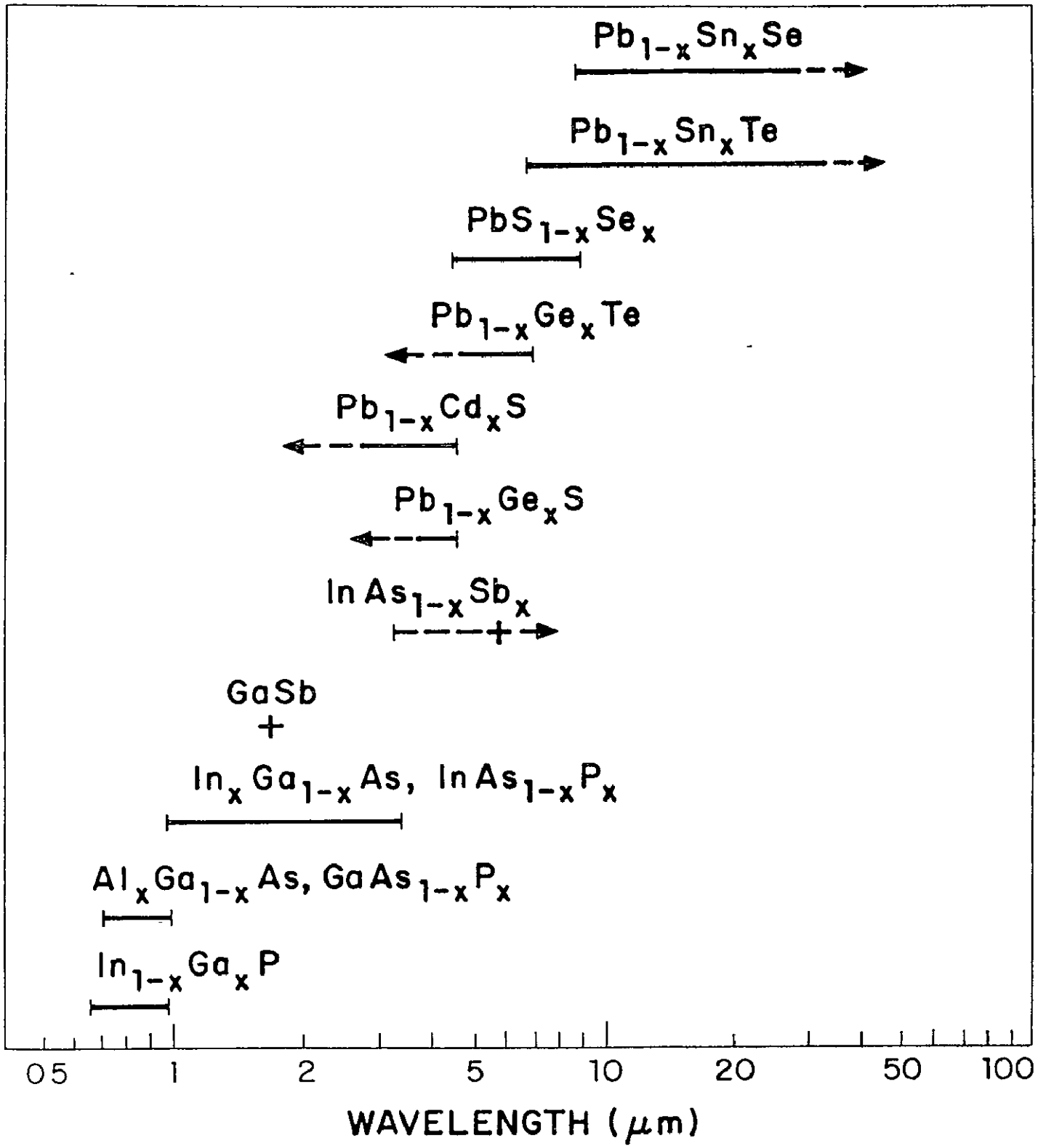
$Pb_{1-x}Sn_xSe$
$Pb_{1-x}Sn_xTe$
$PbS_{1-x}Se_x$
$Pb_{1-x}Ge_xTe$
$Pb_{1-x}Cd_xS$
$Pb_{1-x}Ge_xS$
$InAs_{1-x}Sb_x$
GaSb
+
$In_xGa_{1-x}As$, $InAs_{1-x}P_x$
$Al_xGa_{1-x}As$, $GaAs_{1-x}P_x$
$In_{1-x}Ga_xP$
0.5
1
2
5
10
20
50
100
WAVELENGTH (μm)

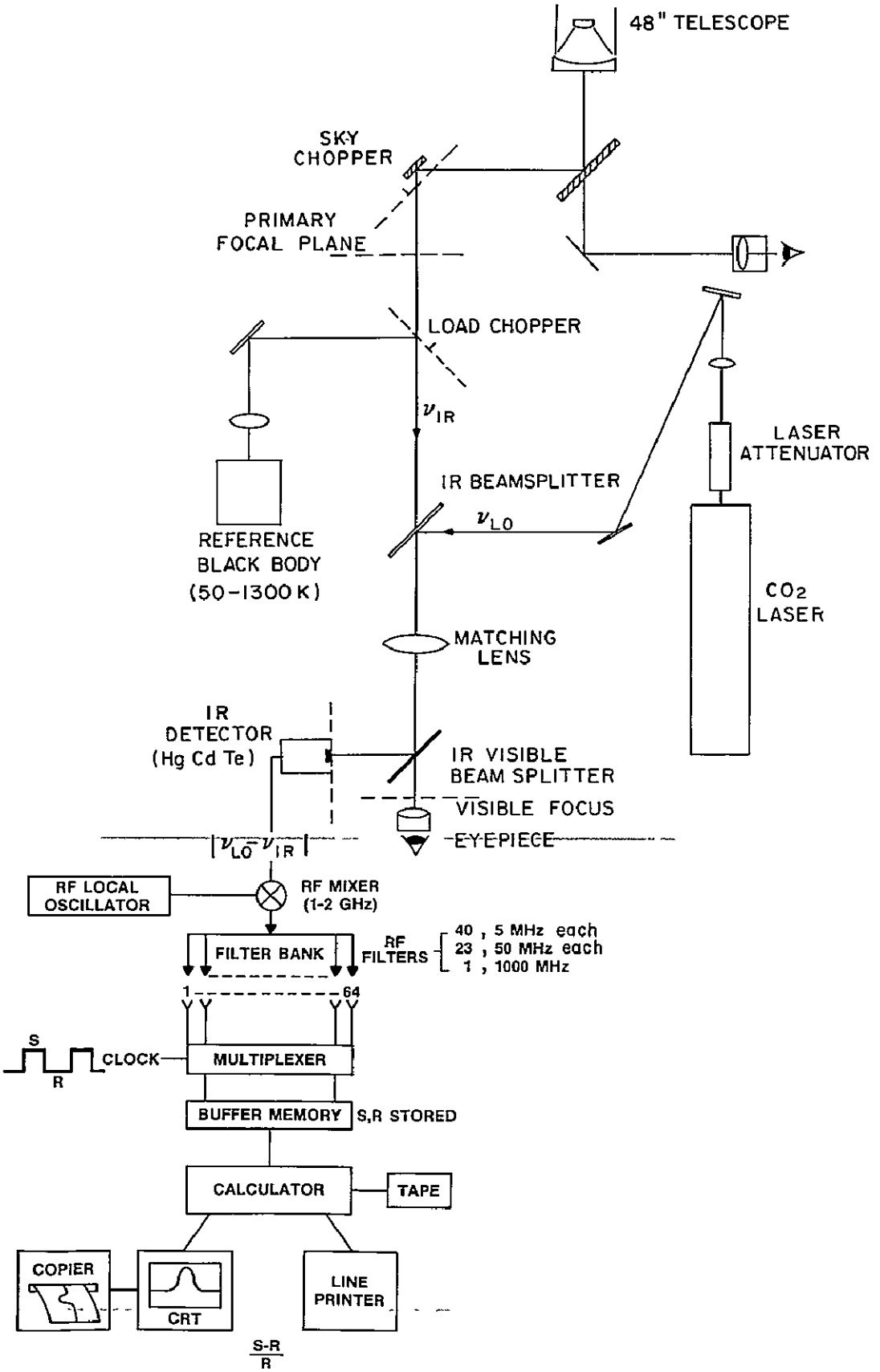
48" TELESCOPE
SKY CHOPPER
PRIMARY FOCAL PLANE
LOAD CHOPPER
ν_{IR}
LASER ATTENUATOR
IR BEAMSPLITTER
ν_{LO}
REFERENCE BLACK BODY (50-1300 K)
CO_2 LASER
MATCHING LENS
IR DETECTOR (Hg Cd Te)
IR VISIBLE BEAM SPLITTER
VISIBLE FOCUS
EYEPIECE
$|\nu_{LO} - \nu_{IR}|$
RF LOCAL OSCILLATOR
RF MIXER (1-2 GHz)
FILTER BANK
RF FILTERS
40 , 5 MHz each
23 , 50 MHz each
1 , 1000 MHz
1
64
S
R
CLOCK
MULTIPLEXER
BUFFER MEMORY
S,R STORED
CALCULATOR
TAPE
COPIER
CRT
LINE PRINTER
S-R / R

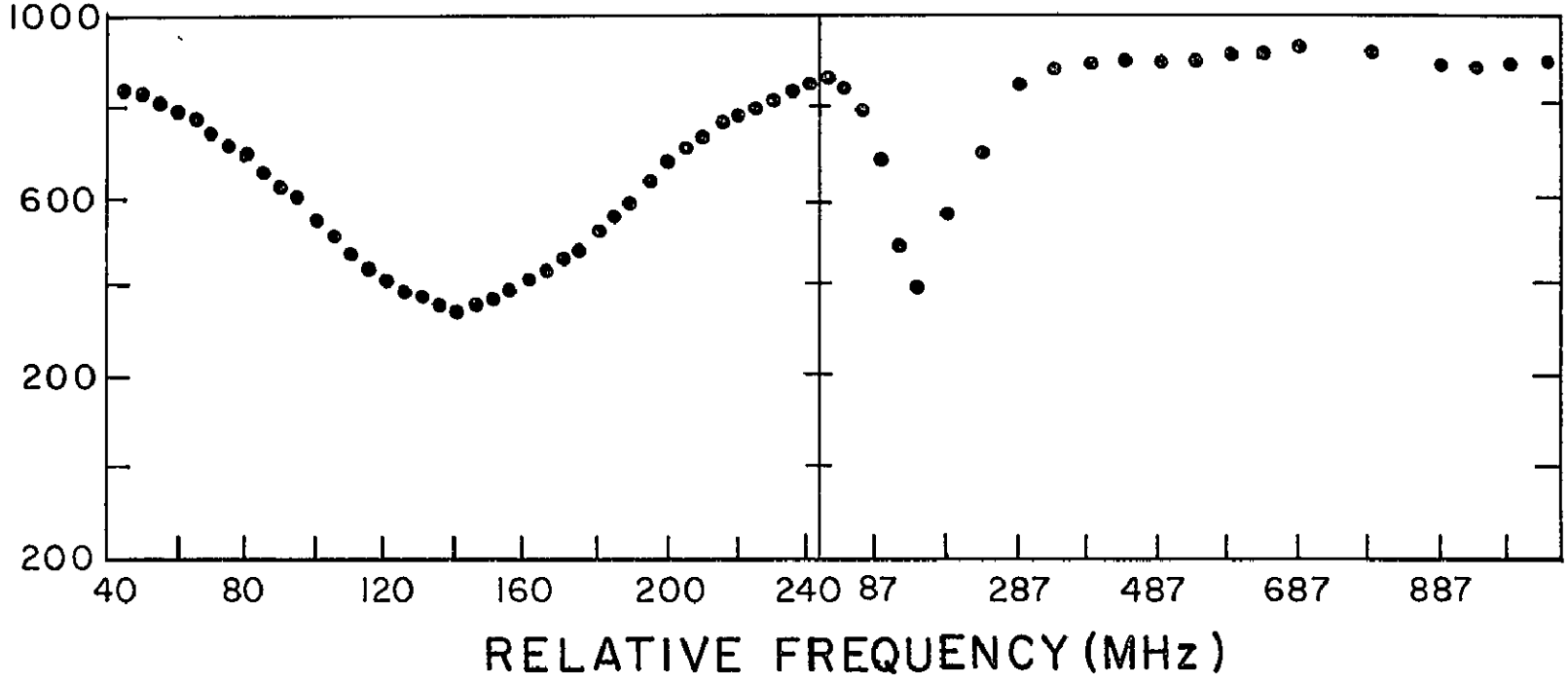
1000
600
200
200
40
80
120
160
200
240
87
287
487
687
887
RELATIVE FREQUENCY (MHz)

Fig. 15. Schematic of laboratory tuneable diode laser absorption spectrometer

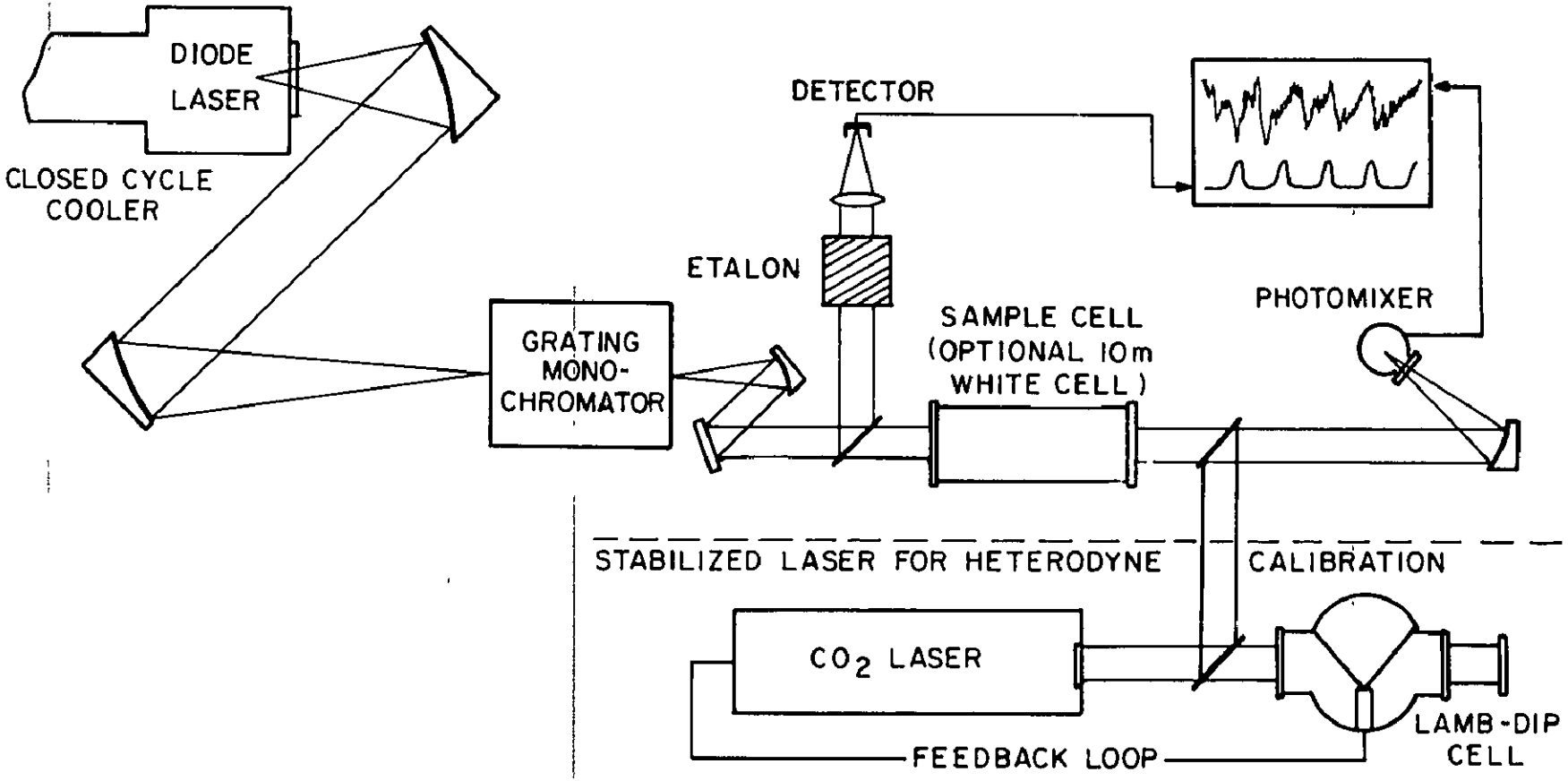

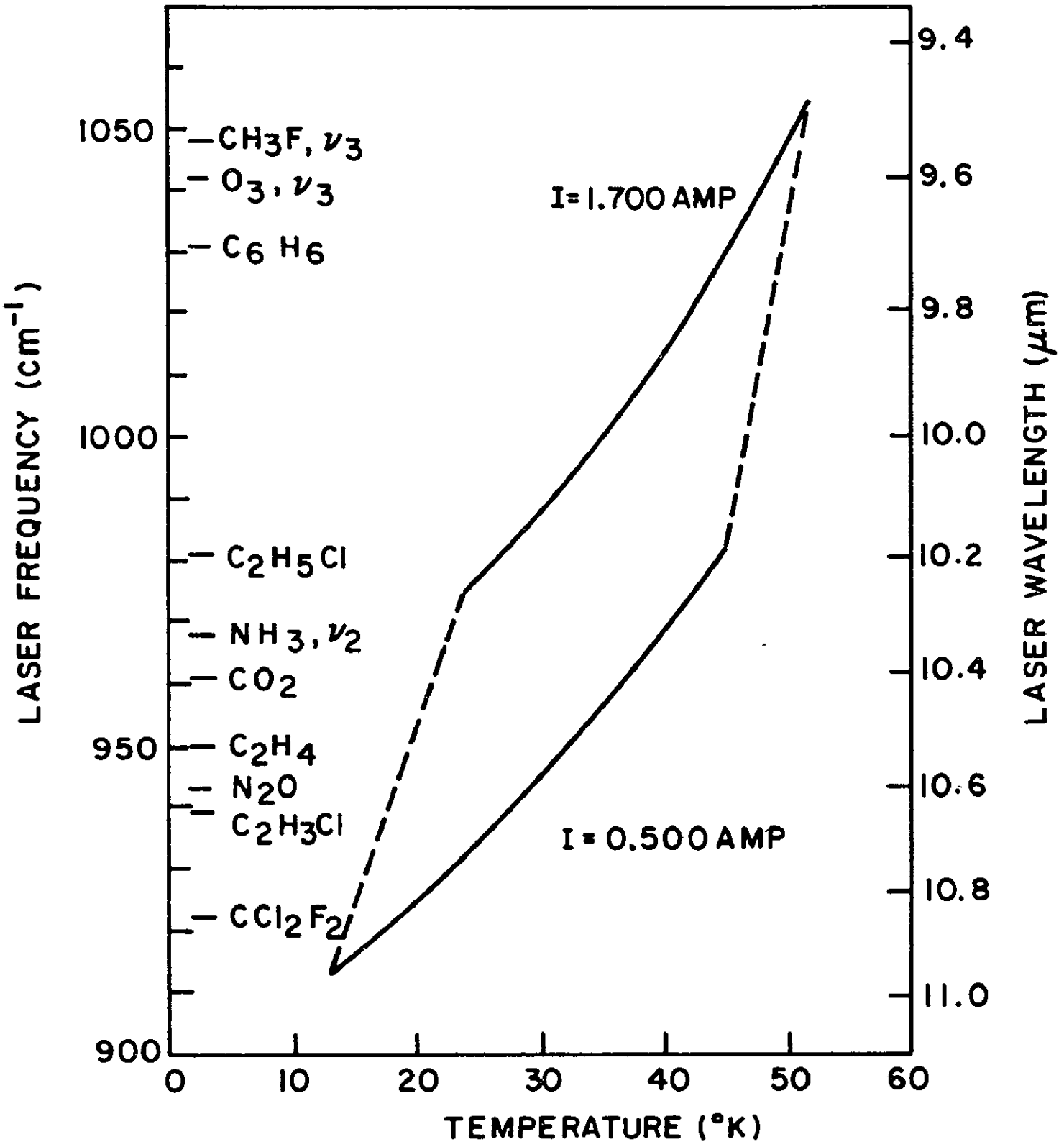
LASER FREQUENCY (cm⁻¹)
LASER WAVELENGTH (μm)
TEMPERATURE (°K)
1050
1000
950
900
9.4
9.6
9.8
10.0
10.2
10.4
10.6
10.8
11.0
0
10
20
30
40
50
60
CH3F, ν3
O3, ν3
C6 H6
C2H5Cl
NH3, ν2
CO2
C2H4
N2O
C2H3Cl
CCl2F2
I=1.700 AMP
I = 0.500 AMP

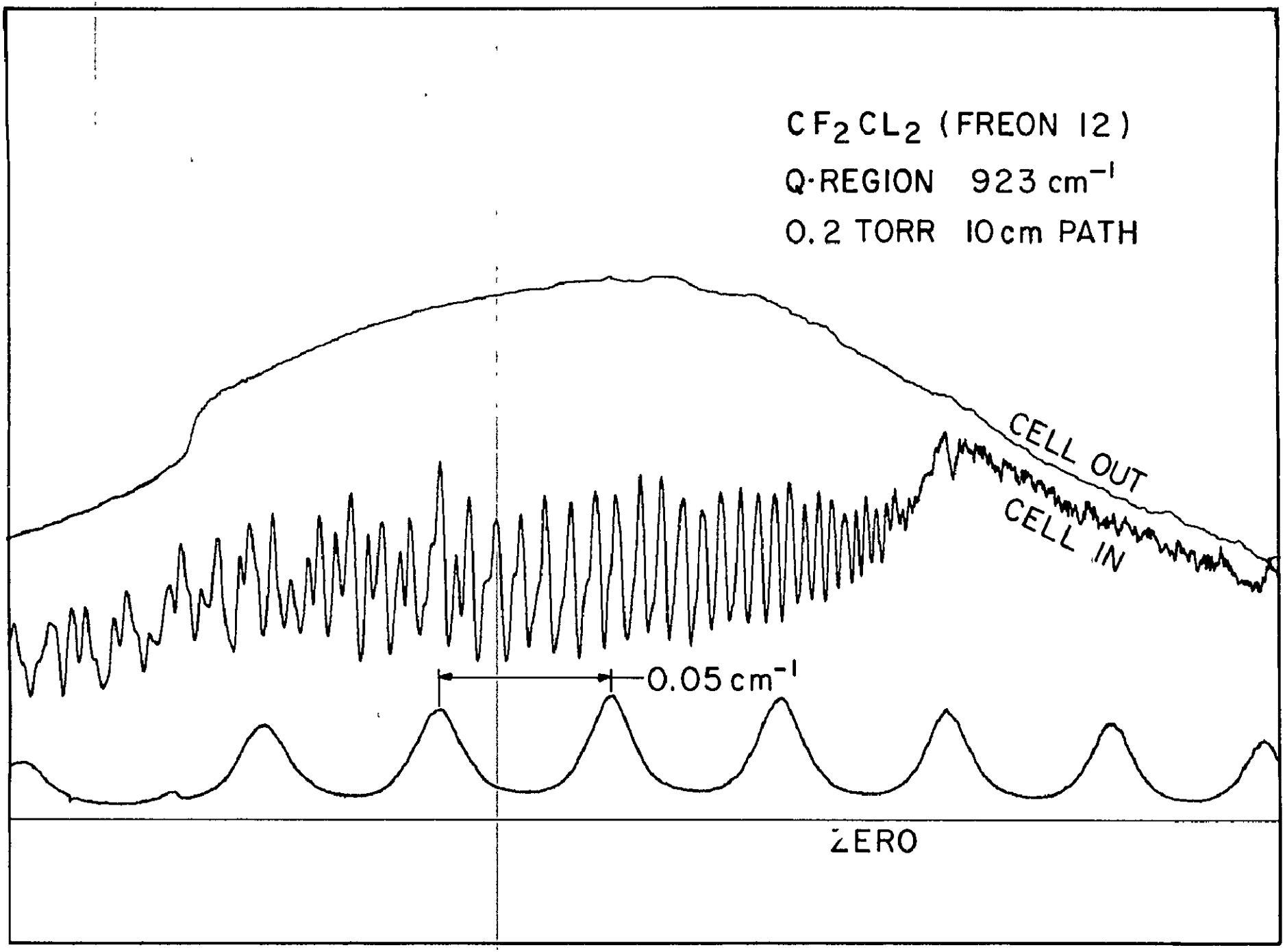
CF_2CL_2 (FREON 12)
Q-REGION 923 cm^{-1}
0.2 TORR 10cm PATH
CELL OUT
CELL IN
0.05 cm^{-1}
ZERO

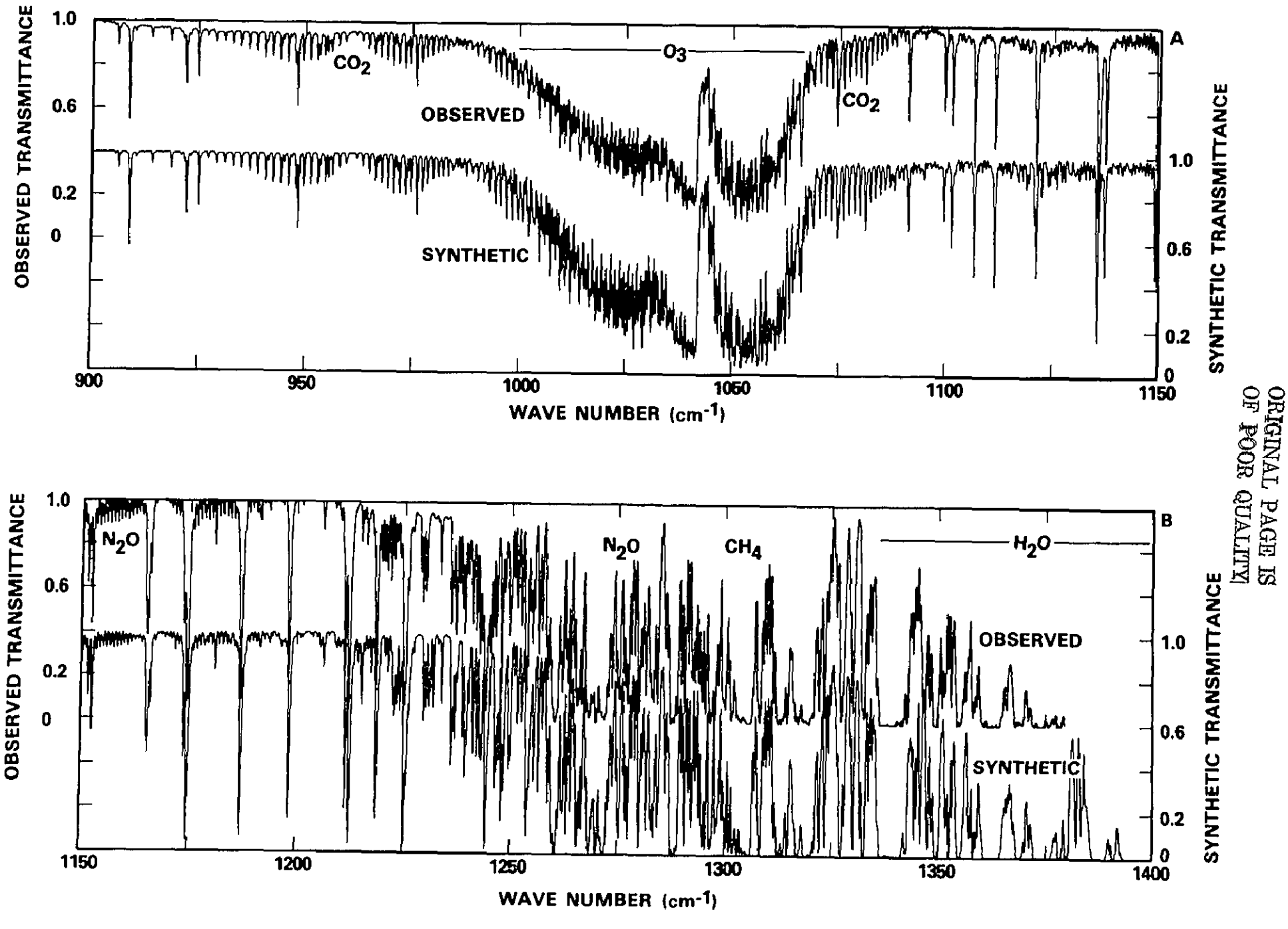

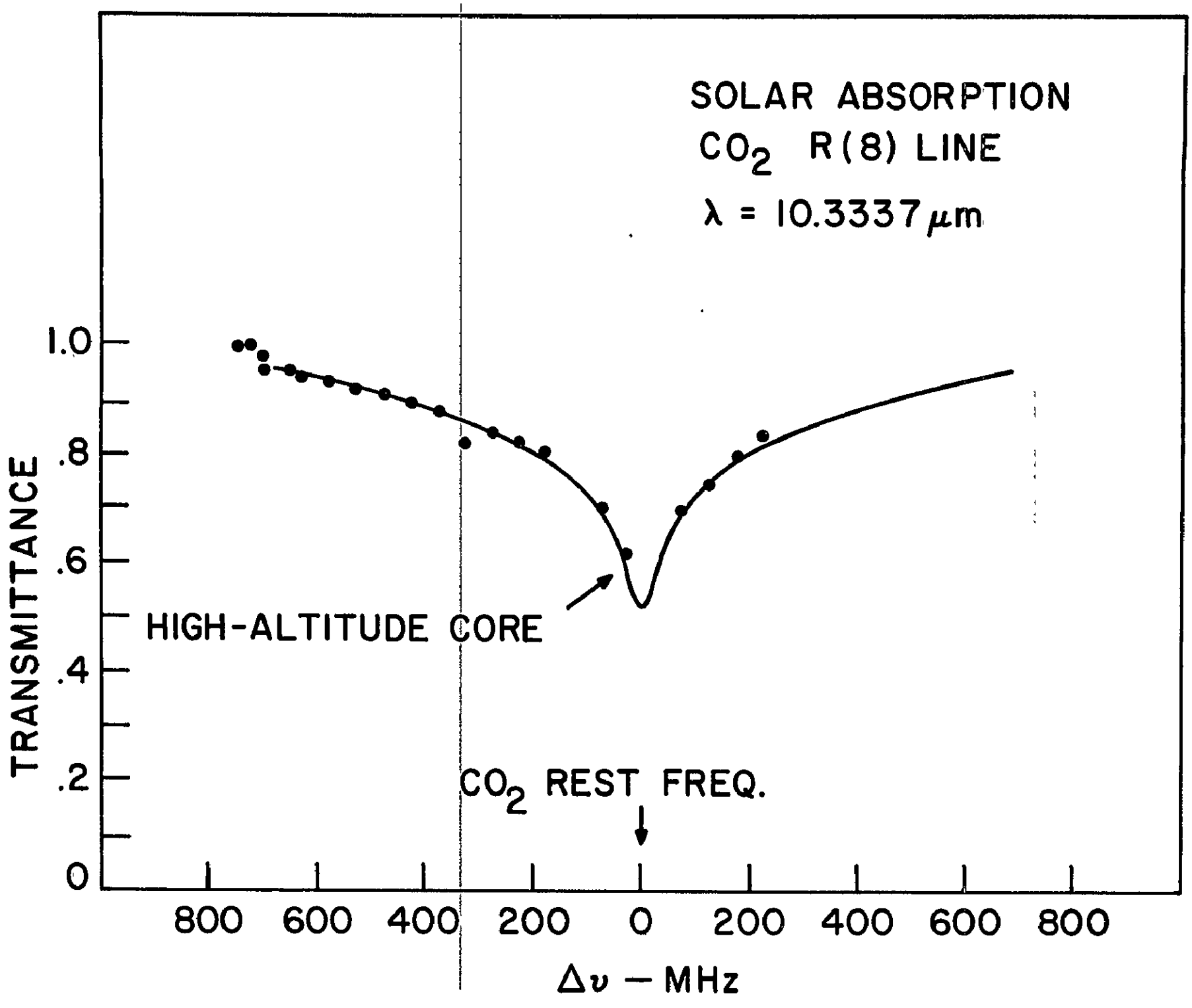
SOLAR ABSORPTION
CO_2 R(8) LINE
λ = 10.3337 μm
TRANSMITTANCE
1.0
.8
.6
.4
.2
0
HIGH-ALTITUDE CORE
CO_2 REST FREQ.
800
600
400
200
0
200
400
600
800
Δν — MHz

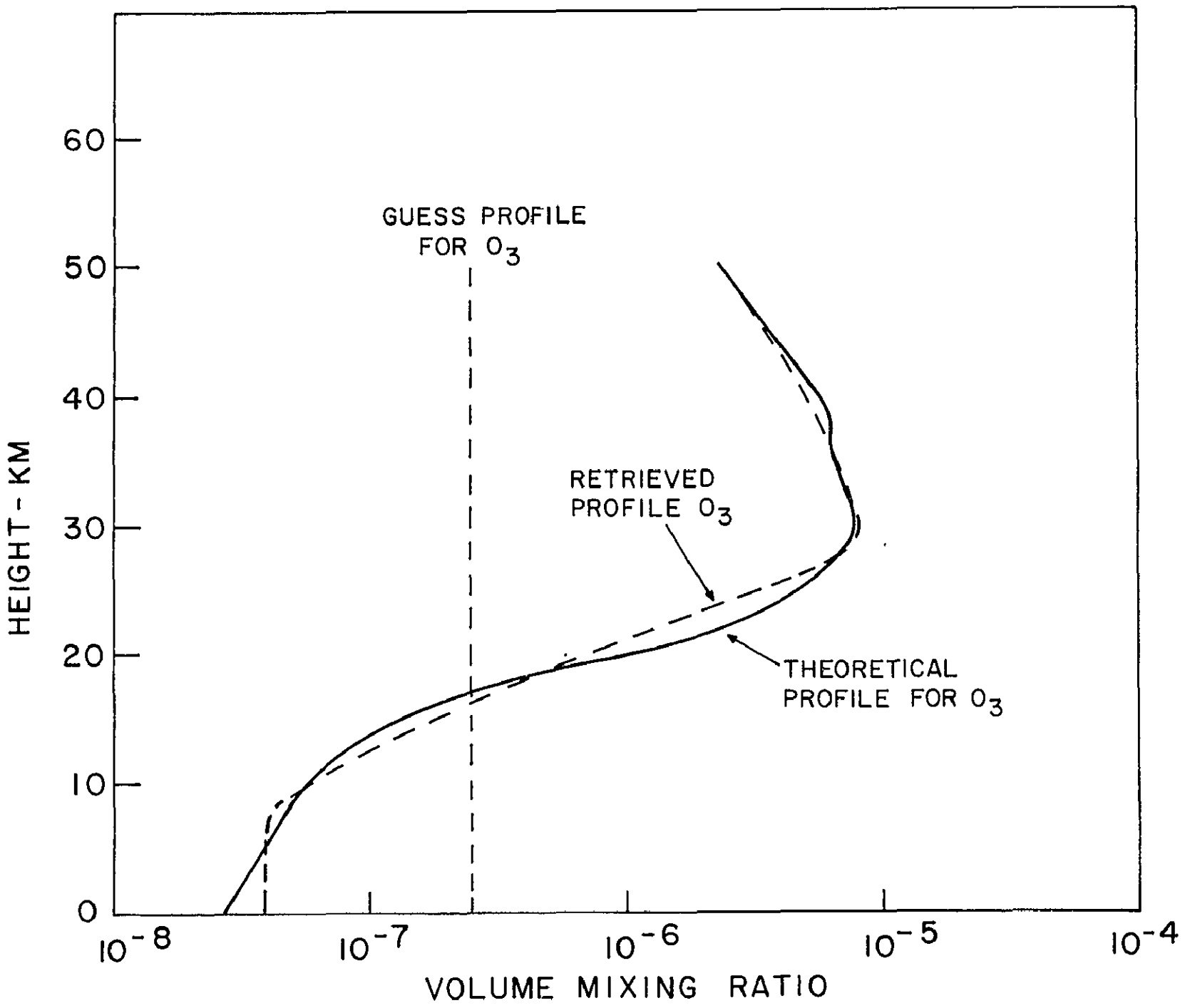
GUESS PROFILE
FOR O_3
RETRIEVED
PROFILE O_3
THEORETICAL
PROFILE FOR O_3
HEIGHT - KM
VOLUME MIXING RATIO
0
10
20
30
40
50
60
10^{-8}
10^{-7}
10^{-6}
10^{-5}
10^{-4}

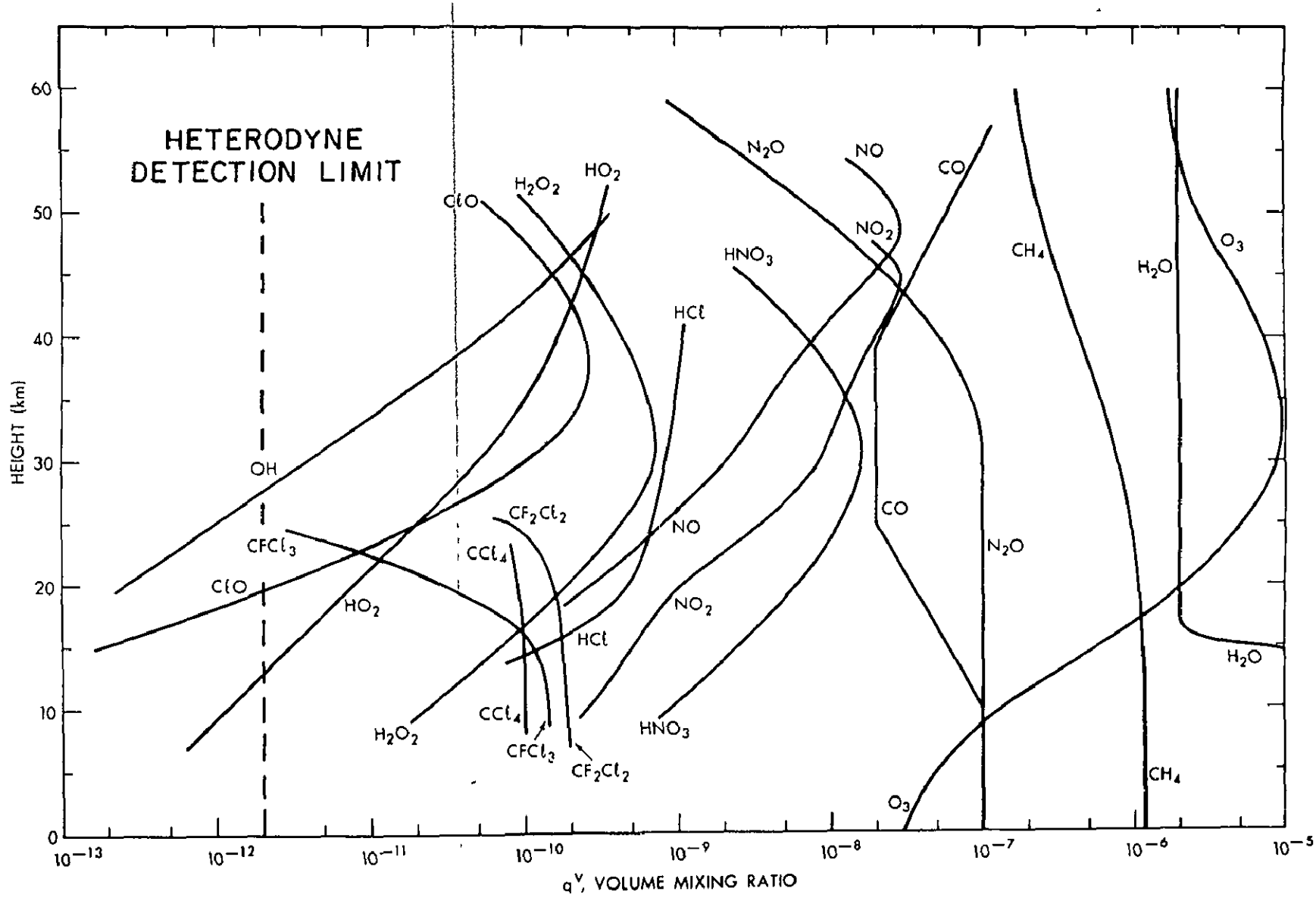
HETERODYNE
DETECTION LIMIT
HEIGHT (km)
60
50
40
30
20
10
0
OH
ClO
HO2
H2O2
CFCl3
CF2Cl2
CCl4
HCl
NO
NO2
HNO3
N2O
CO
CH4
H2O
O3
10−13
10−12
10−11
10−10
10−9
10−8
10−7
10−6
10−5
qV, VOLUME MIXING RATIO

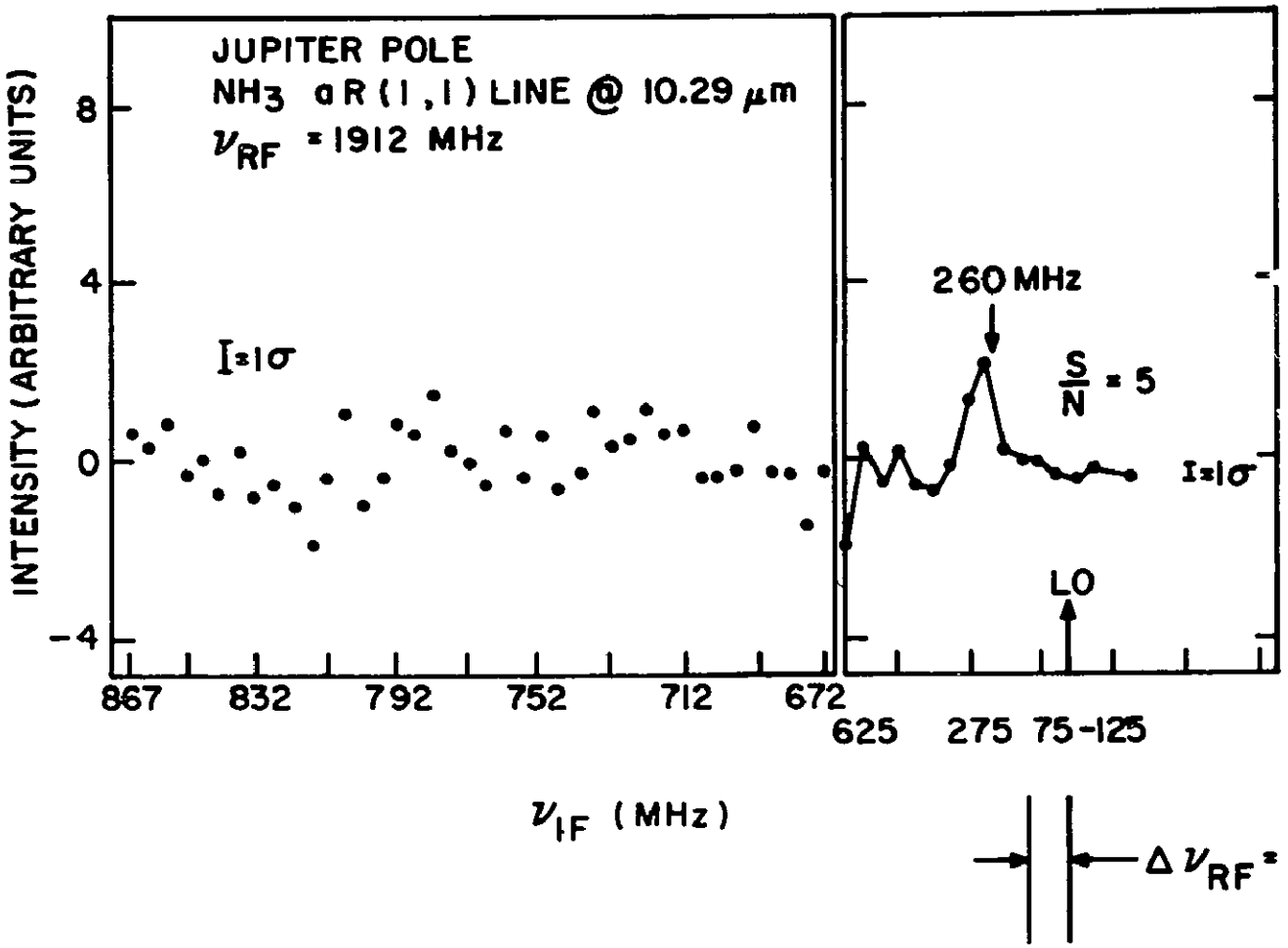

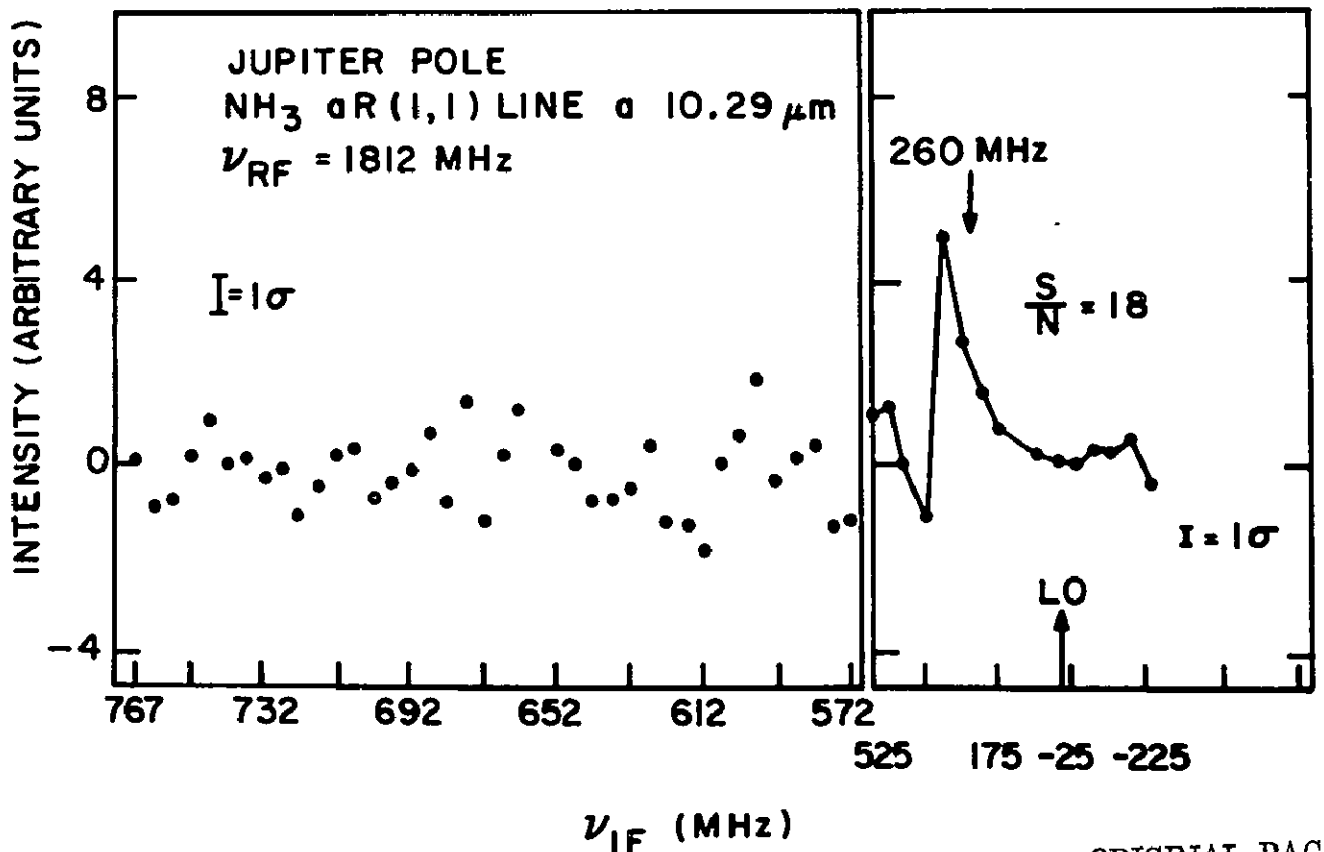

BIBLIOGRAPHIC DATA SHEET

1. Report No	2. Government Accession No.	3. Recipient's Catalog No.
4. Title and Subtitle High Resolution Infrared Spectroscopy: Some New Approaches and Applications to Planetary Atmospheres		5 Report Date 6 Performing Organization Code
7. Author(s) Michael J. Mumma		8. Performing Organization Report No.
9 Performing Organization Name and Address NASA/Goddard Space Flight Center Greenbelt MD 20771		10. Work Unit No 11. Contract or Grant No
12. Sponsoring Agency Name and Address		13. Type of Report and Period Covered 14 Sponsoring Agency Code
15 Supplementary Notes		

16 Abstract Recent advances in tuneable infrared lasers and in infrared heterodyne spectroscopy enable sub-doppler spectroscopy of laboratory gases and planetary atmospheres. In this paper, the principles of spectral line formation and of techniques for retrieval of atmospheric temperature- and constituent-profiles are discussed. Applications to the atmospheres of Earth, Mars, Venus, and Jupiter are illustrated by results obtained with Fourier transform and infrared heterodyne spectrometers at resolving powers $(\lambda/\Delta\lambda)$ of $\sim 10^4$ and $\sim 10^7$, respectively, showing the high complementarity of spectroscopy at these two widely different resolving powers. The principles of heterodyne spectroscopy are reviewed and its applications to atmospheric probing and to laboratory spectroscopy are discussed. Direct absorption spectroscopy with tuneable semiconductor lasers is discussed in terms of precision frequency-and line strength-measurements, showing that substantial advances in laboratory infrared spectroscopy are at hand.

17. Key Words (Selected by Author(s))	18. Distribution Statement		
19 Security Classif. (of this report)	20. Security Classif. (of this page)	21 No of Pages	22. Price*

*For sale by the National Technical Information Service, Springfield, Virginia 22151